JANUARY 2021 M.Sc. in Aircraft and Aerospace Engineering MERT KESİKMİNARE

REPUBLIC OF TURKEY

GAZİANTEP UNIVERSITY

GRADUATE SCHOOL OF NATURAL & APPLIED SCIENCES

THERMAL FATIGUE CHARACTERISTICS OF FIBER-REINFORCED COMPOSITE MATERIALS

M.Sc. THESIS

IN

AIRCRAFT AND AEROSPACE ENGINEERING

BY

MERT KESİKMİNARE

JANUARY 2021

THERMAL FATIGUE CHARACTERISTICS OF FIBER-REINFORCED COMPOSITE MATERIALS

M.Sc. Thesis

in

Aircraft and Aerospace Engineering

Gaziantep University

Supervisor

Assoc. Prof. Dr. Eyüp YETER

by

Mert KESİKMİNARE

January 2021

I hereby declare that all information in this document has been obtained and presented in accordance with academic rules and ethical conduct. I also declare that, as required by these rules and conduct, I have cited and referenced all material and results that are not original to this work.

Mert KESİKMİNARE

ABSTRACT

THERMAL FATIGUE CHARACTERISTICS OF FIBER-REINFORCED COMPOSITE MATERIALS

KESİKMİNARE, Mert
M.Sc. in Aircraft and Aerospace Engineering
Supervisor: Assoc. Prof. Dr. Eyüp YETER
January 2021
54 pages

The material of the fiber and matrix of fiber-reinforced laminated composite materials directly influences the mechanical performance of a composite. Fibers are generally expected to have high elastic modulus and strengths. The combination of polymer matrix composites with different materials at the macroscopic level affects its strength against thermal loads. Moreover, the most important design criterion may be the resistance of these materials to thermal loads. In addition, these loads can be repeated due to the needs of the usage areas. Especially in the aviation industry, resistance to repetitive thermal loads is very important in the design of aerospace vehicles. In this thesis, it is aimed to understand behavior of Glass/Epoxy, Graphite/Epoxy, and Boron/Epoxy polymer matrix composites under the thermal fatigue loads. $[(0/90)_2]_s$, $[(15/-75)_2]_s$, $[(30/-60)_2]_s$, and $[(45/-45)_2]_s$ fiber orientations and ply sequences are used. Effects of two different boundary conditions, cutouts, and position of these cutouts are also researched.

Keywords: Fiber-reinforced Composites, Thermal Fatigue, Finite Element Analysis,

ÖZET

ELYAF TAKVİYELİ KOMPOZİT MALZEMELERİN TERMAL YÜK ALTINDAKİ ÖZELLİKLERİ

KESİKMİNARE, Mert
Yüksek Lisans Tezi, Uçak ve Uzay Mühendisliği
Danışman: Doç. Dr. Eyüp YETER
Ocak 2021
54 sayfa

Elyaf takviyeli tabakalı kompozit malzemelerde kullanılan elyafın ve matrisin malzemesi bu kompozitin mekanik performansını doğrudan etkiler. Elyafların genellikle yüksek elastik modül ve mukavemetlere sahip olması beklenir. Polimer matriks kompozitlerin doğası gereği, makroskopik düzeyde farklı malzemelerin birleşiminden oluşmasından dolayı termal yüklerden oldukça etkilenirler. Bu malzemelerin ısıl yüklere karşı direnci bazen en önemli tasarım kriteri olabilir. Ayrıca kullanım alanlarının ihtiyaçları nedeniyle bu malzemeler tekrarlı yüklere sıklıkla maruz kalmaktadırlar. Özellikle havacılık endüstrisinde, hava ve uzay araçlarının tasarımında tekrarlanan termal yüklere karşı dayanım önemlidir. Bu tezde, Cam / Epoksi, Grafit / Epoksi ve Bor / Epoksi polimer matris kompozitlerin ısıl yorulma yükleri altındaki davranışının araştırılmıştır. $[(0/90)_2]_s$, $[(15/-75)_2]_s$, $[(30 / -60)_2]_s$ ve $[(45/-45)_2]_s$ fiber yönelmeleri kullanılmıştır. Ayrıca, İki farklı sınır koşulunun, plakaya açılan kesitlerin ve bu kesiklerin konumu da araştırılmıştır.

Anahtar Kelimeler: Elyaf-takviyeli Kompozitler, Termal Yorulma, Sonlu Eleman Analizi

"Dedicated to my family"

ACKNOWLEDGEMENTS

I would like to express my debt of gratitude to Assoc. Prof. Dr. Eyüp YETER for his generosity, guidance, advice, expertise, understanding encouragements, insight, and suggestions throughout the research and preparation of this thesis. It was a pleasure and honor to work with him. Words can never be enough to thank your kindness. I would like to express my love and gratitude to my family for their support, always best wishes. I offer my humblest thanks to my family, grandmother, grandfather, and mother.

TABLE OF CONTENTS

LIST OF TABLES

LIST OF FIGURES

CHAPTER 1

INTRODUCTION

1.1 Introduction

Today's engineering has evolved to design structures resistant to different types of loads and to develop materials suitable for these designs. Polymer matrix composites have become the most important choice for researchers with their many superior features. Especially, high specific modulus and strength, and dimensional stability during large changes in temperature in space make the polymer matrix composites the material of choice in space applications. However, composite materials have some disadvantages besides their superior properties. The strength of composite materials against repeated loads is important in this context and has been investigated by many researchers.

The material of the fiber and matrix of polymer matrix composites directly influences the mechanical performance of a composite. Fibers are generally expected to have high elastic modulus and strengths. Due to the nature of polymer matrix composites, due to the combination of different materials at the macroscopic level, they are highly affected by thermal loads. Sometimes, perhaps the most important design criterion may be the resistance of these materials to thermal loads. Also, these loads can be repeated due to the needs of usage areas. Especially in the aviation industry, resistance to repetitive thermal loads is very important in the design of aerospace vehicles.

Thermal fatigue can be defined as the exposure of structures or materials to repeated thermal loads. These thermal loads can be above zero degrees, below zero degrees, or a temperature below zero to a temperature above zero. For instance, satellite structures should be dimensionally stable in space during temperature changes between –165 °C and 100 °C.

In this study, the algorithm previously created by Yeter [1,2] has been adapted on composite materials. This algorithm, the details of which will be given in chapter 3, can be applied to structures under different boundary conditions and different

repeated loads. The prepared algorithm has been analyzed using the ANSYS mechanical APDL module.

1.2 Scope of the Thesis

Thermal load causes different types of damage to the material. These damages start with the formation of cracks and cannot be predicted in this material during design step. This effect can cause more effective damages especially in composite material consisting of matrix and reinforcement element which have different thermal expansion coefficients. Also, the repetition of this thermal load between plus and minus temperatures further increases the significance of this effect.

In this sense, the scope of this thesis is to search the thermal fatigue characteristics of polymer matrix composites under various boundary conditions. In the study, the effects of different fiber orientations and materials on the thermal fatigue strength were investigated. In addition, the effect of stress concentration (opening a cut-out) was examined.

General information on definition and importance of thermal fatigue behavior of polymer matrix composites given in chapter 1. Aims and objectives of the thesis and main contributions of the thesis are also emphasized in this chapter. Literature on the thermal fatigue of composite materials is given in Chapter 2. Thermal fatigue algorithm for polymer matrix composites and details of the algorithm are given in chapter 3. Results of discussions of the thesis are given in chapter 4. General conclusion is given in chapter 5.

1.3 Aims and Objectives of the Thesis

The main purpose of this thesis is to investigate thermal fatigue resistance of polymer matrix composites under the thermal fatigue loading. the algorithm previously created by Yeter [1,2] has been adapted on composite materials. Effects of different fiber orientations and materials on the thermal fatigue strength were investigated. In addition, the effect of stress concentration was examined.

In this thesis, it is aimed to understand behavior of polymer matrix composites under the thermal fatigue loads. In the first part of the study, the algorithm was adapted to polymer matrix composite. In the second part of the study, different cases were

formed and these cases are applied to polymer matrix composites. $[(0/90)_2]_s$, $[(15/-75)_2]_s$, $[(30/-60)_2]_s$, and $[(45/-45)_2]_s$ fiber orientations are used. Glass/Epoxy, Graphite/Epoxy, and Boron/Epoxy are used as material types. Effects of thermal fatigue on the Glass/Epoxy, Graphite/Epoxy, and Boron/Epoxy have been investigated. Then, the results were compared.

1.4 Main Contributions of the Thesis

In this study, thermal fatigue behavior of polymer matrix composites was investigated numerically. The adapted algorithm for polymer matrix composites was used. The main novelties of this thesis are:

- To adapt the thermal fatigue algorithm for polymer matrix composites.
- To investigate effects of different fiber orientation angles on the thermal fatigue resistance.
- To identify effects of different fiber types on the thermal fatigue resistance.
- To evaluate the effects of cutouts and their positions on the thermal fatigue loads for composite materials.

CHAPTER 2

LITERATURE SURVEY

2.1 Introduction

In this section, an overview of thermal fatigue studies on materials, thermal fatigue damages and literature review on the calculation of these damages will be presented.

2.2 Studies Related to Thermal Fatigue

Yeter [1, 2] studied the effects of thermal fatigue in 2014, 2024, 6061, and 7075 aluminum alloys, which are more widely used in the aviation industry. In the ANSYS program, an algorithm has been developed to examine the behavior of materials exposed to repeated thermal loads. The main purpose here is to examine the exposure of aluminum alloys used in the aviation industry to thermal load, particularly structures used on the exterior part of aircraft. The effects of thermal fatigue on different riveting parameters such as rivet size, rivet edge distance, rivet spacing were investigated [2].

Yeter and Ozer [3] studied on thermal fatigue characteristics of Plates with Cutouts. It was shown that cut-outs directly effects thermal fatigue resistance.

Özer [4] investigated the effects of thermal loads to plates. The resistances of isotropic thin plates under the thermal fatigue loads are searched. Different aluminum alloys are investigated and it was obtained that material type and boundary conditions have high effect to the thermal cyclic loads.

Tian et al. [5] examined the thermal and mechanical shock resistance of the newly produced Si3N4 / (W, Ti) C ceramic material by taking the sections after quenching with water, respectively. While the strength after quenching began to decrease regularly as the bending strength retained, then the graph continued unevenly. The critical temperature point is 600 ° C for graded products and 500 ° C for homogeneous products. After the formation of micro-cracks and the merging of the ongoing cracks, the irregularity in the strength curve was revealed and clear curves were formed. Micro-cracks and small chipping were observed in the vehicle

failure mechanisms. Abrasions occurred on the lateral surfaces of the materials that received the same number of impacts. It has been observed that the surface layer of materials due to thermal shock tensile stress changes. The gradually formed material can relieve the clamping stress, thermal and mechanical stress. Also, preventing the formation of micro-cracks also prevents the formation of thermal shock and stress.

Wu et al. [6] investigated thermal fatigue, crack propagation, and fracture formation and investigate the thermal differences between the special aluminum alloy containing 65% SiCp and other alloys. Products with a V-shaped dashed line were observed with line breaks and tip cracks after cycle thermal shock at the time determined by water quenching from 300 ° C. Examination of the fracture surface resulted in the initiation and propagation of thermal fatigue cracking of such a composite. That larger reinforcement particles in the composite could be broken more easily by thermal shock. Reducing the size of the added particles has helped to increase the resistance of this type of composite against thermal fatigue. Besides, it has been shown that the reduction of the new product size created by additional particles increases the resistance of the composite to thermal fatigue.

Li et al. [7] studied thermal fatigue coefficients and mechanical properties of metal fiber laminates (FML) produced using aluminum and lithium. As a result, it was stated that AL-LI FMLs exposed to approximately one thousand cycles had significant strength problems and many defects were observed. It was noted that the samples taken to the test were more stable than the produced FMLs and had excellent laminar properties. It was observed that the thermal resistance of FMLs produced with aluminum-lithium materials increased. Also, after thermal fatigue treatments, fatigue and crack growth coefficients were closely observed when compared to the method by which new AL-LI FMLs were produced. Small changes in the properties of aluminum-lithium layers did not make a big difference when considering material strength, thermal strength, and strength.

Mei et al. [8] investigated the differences in the thermal strength and fatigue coefficient of fiber-reinforced SiC matrix composites produced by the chemical vapor infiltration method (polymer coating technique). Many factors on the dynamically tested C / SiC composites were investigated and a record has been requested. During the test, the results of dynamic damages, tensile modulus (UTS), and SEM were evaluated. As a result, it has been observed that the weakest formation for 2D C / SiC composites thermally under different atmospheres of the

products decreases as the atmospheric humidity increases, the dynamic load applied to the products, and the deterioration rate of the composites can increase. In addition, analyzes and records were arranged with SDIA, and requested graphics were taken. The changes in the composite materials produced were observed depending on the tested environment, dynamic load, and humidity.

Longbiao et al. [9] examined the behavior and strength of C / SiC composites at different room temperatures of 3 different fiber preforms formed after the cross and single-part production schemes. Poisson shrinkage and the fiber volume ratio of the produced material fibers, peak stress points, and the sudden and new developments caused by the active parameters of C / SiC composites depending on the conditions tested were examined. The fiber volume fraction in the loading direction, high-temperature oxidation, and interfacial shear formation between fiber and matrix during stretching was recorded and studied.

Sarasini et al. [10] investigated the new material is woven aramid and basalt fabrics were created using special resin and then their strength after the impacts were applied. The strengths of Aranid / basalt hybrid laminates, which were created using various synths, were investigated depending on flexural coefficient after the impacts were applied. The tensile test results were observed together for the evaluations after the damage occurred. As a result, hybrid laminates formed with specially designed arrays contain better impact energy than all aramid laminates and comply with the previously specified damage tolerance, and the configuration predicts that basalt and hybrid laminates are more preferred and should be used in sandwich-shaped structures.

Kobayashi et al. [11] observed microscopic damage changes in high-temperature CFRP, AS4 / PEEK cross-layer laminates under thermal cycling. After varying layer thicknesses, two different laminates were tested with special desired arrangement shapes. The number of cycles was applied 90 times and micro-cracks started in the applications. The cracks that occurred continued to increase steadily after 90 tests. During the evaluation procedures, a damage mechanical analysis was recorded following the rules to examine the energy release coefficients and thermal stress values of cracks. Some improvements have also been made to the Paris law.

Bieniaś and Dadej [12] examined fiber metal laminates in 3 different stages fatigue formation, crack formation, and mechanical breakage on environmental factors and mechanical loads. Completely deterioration of the materials is expected. As a result,

it is concluded that the specified static strength and fatigue life differ as a result of the stress cycle curve being formed by different sequences.

Shan et al. [13] studied the thermal fatigue behavior and thermal resistance of Si - Mo - Cr coated C / C composites coated by C / Interface Polymerization method. To change the thermal coefficient and strength of the composite material produced, the carbon-carbon (C / C) composites have been processed and the specified applications have been achieved. The resistance of the coated materials in thermal fatigue was simulated and presented as a document. The products, which were tested at room temperature and 15 times, lost mass in two different products. Thermal fatigue properties of the pre-oxidized samples were observed in the C / C interface polymerization, the Si-Mo-Cr coating, and the C / C substrate, and resulted in shrinkage in the crack lengths formed.

Yan et al. [14] investigated the formed plane internal shear strength (IPSS) of the material (C / SiC) of 2D carbon fiber reinforced silicon carbide composite and the cuts in the form of double lines were intended to be used at room temperature under a certain load. As a result, compression of the DNS is known to be very effective in measuring the IPSS of the C / SiC. It was determined that the temperature factor of IPSS was important for C / SiC. It has been determined that IPSS will increase up to a certain point as the temperature increases and then continue regularly. Also, the matrix fracture caused by the shear load acting and the resulting fractures and failures created cut slits in the products formed.

Tian et al. [15] examined the proper temperature and conditions that were taken into consideration during the formation of nano monolithic Si3N4 and Si3N4 - TiC nanocomposites. After the formation of monolithic Si3N4 nano-ceramic and Si3N4 - TiC nanocomposites, the quenching process applied with water was used to examine the specified thermal behavior, and fatigue coefficients were examined and recorded. It has been determined that Si3N4 - TiC nanocomposites have higher resistance at their critical temperature and strength than monolithic silicon nitride nano-ceramics. The product with the best strength among the produced products was recorded and plotted as 550 C 'obtained from Si3N4 - TiC nanocomposite with the addition of 10% TiC.

Zheng et al. [16] studied on composite materials Sialon - Si3N4 ceramics. The production was ensured by pressing following the values specified in the ambient temperature. The general properties and resistance coefficients of ceramic-formed

products were examined. Sialon - Si3N4 products were quenched by using water. While the results were examined that the thermal resistance and static strength and strength of the graded ceramic were higher compared to the homogeneous reference, it was observed that the thermal resistance coefficient of the graded ceramic was higher. The critical temperature difference was approximately 600 ° C in the products created. The crack resistance graphs and the examination details of micro-crack structures of the tested materials in ceramic structure and homogeneously used are given.

Colombo et al. [17] investigated the innovations and designs in composite materials continue, one of the most striking materials is basalt reinforced composite materials. Some fibers used to increase the strength are not preferred due to cost reasons and glass fibers are generally preferred instead of carbon fiber. Structurally, the arrangement diagram of basalt reinforced composites is very important. In this study, it was requested to obtain and examine the fatigue schemes experimentally. In the experimental study, the thermal responses to the loads were also evaluated by thermography. The thermal fatigue mechanical strength of basalt reinforced composite materials formed as a result of the studies and will help to examine all of the general problems.

Wong [18] studied the thermal expansion in products applied using sandwich sequencing and the solutions that can be created. In the first solution step, the strength of the cracks formed throughout the whole layer can be seen as elastic, with zero lateral stiffness considered to be equivalent to those of soldered ones. Interfacial shifts and interfacial separations applied consecutively at a high order frequency level were investigated. Second, the interfacial stresses are integrated into the forces and the modification of the average shear stress is studied using the sequential frequency function. As a result of the examinations, the strength coefficients of the studies, strength schemes, and all solution-oriented stages with the necessary regulations are specified in the thesis.

Chen et al. [19] investigated ZrB2-SiC-graphite composite thermal resistance coefficient, heat resistance conditions, and surface temperature distribution, taking into account the strength ranges, 30, 40, 50, and 60 MPa tests and tensile tests. The sample was plotted by examining the thermal resistance and thermal cycles starting from room temperature up to 2000 ° C under the σ0 constant. As the total strength increases, the thermal fatigue life decreases, micro-cracks, micro crack

morphologies, and all of them are given the figural diagrams. As a result of the investigations, it has been observed that the micro-cracks formed from the strength value may show variability, larger cracks, or fractures with thermal temperature differences. The thermal fatigue life applied by thermal cycles between 25 ° C and 2200 ° C under different σ0 was also tested, and the thermal fatigue coefficient and life were determined below as a result of the investigations.

The fiber/matrix interface shear stress and fatigue behavior of composite materials (CMCs) reinforced with reinforcing fibers were investigated by Longbiao [20]. Fiber composite products with three different arrays were aimed to investigate the interface shear and shear stress, different behaviors, and energy losses of the CMC under room conditions. Increasing fatigue and thermal continuity of behavior were analyzed. When the interface shear stress state decreases in the resulting products, the fatigue hysteresis energy occurs at the highest levels in value and then provides a rapid decrease. This formation coincides with the definition of interface shift and indicates the occurrence of interface shift. The values taken in the case of slip were analyzed numerically. The shear stress trend of fiber preforms and their effects during bending were examined.

Zhou et al. [21] examined the thermal thermal strength of the composite materials used to obtain results. The strength and heat resistance properties of materials reinforced with Al2O3 particles have been investigated. The suitability of a pure molybdenum plate to be tested at 900 degrees has been used. Products applied at 1200 degrees have faster-cracking stress coefficients and the thermal fatigue resistance of composite molybdenum plate is lower than products produced without additives.

Kobayashi et al. [22] investigated high-temperature-resistant carbon fiber reinforced products that have been manufactured and tested to investigate the macroscopic behavior of laminates and their macroscopic damage progression in detail. The preferred materials were intended to be used as thermoplastic polyetheretherketone, AS4 / PEEK and thermoset point based G40-800 / 5260. The use of arrays in various forms has been applied to observe the progression and progression of microscopic injuries. The resulting damages were evaluated using an optical microscope machine and an X-ray radiography machine. In terms of energy release in transverse cracking event, variational analysis was taken into consideration. The modified Paris law was used during the formation of wide cracks. When the data of the mechanical fatigue

test were examined, the rate of transverse crack accumulation under thermal fatigue loading was more in the same energy release rate range. large graphics were recorded and analyzed.

Pan et al. [23] studied thermal behavior of the composites consisting of SiCp / A356, which is the mixture components of the composite material used, during cracking and notch formation. When examining the thermal fatigue behavior, products with V-shaped line-shaped notches were used. The use of an optical microscope (OM) and scanning electron microscope (SEM) was provided due to the desire to see microscopic crack details. It was concluded that the crack formation started to form from the edge after cooling rather than at high temperatures. It was recorded that as the thermal cycles continued, cracking events increased and were detailed. This shows us that the thermal fatigue coefficient has been observed to play an important role in preventing crack propagation. While the hardness of the materials used was inversely proportional to the number of cycles, it was clearly recorded that it decreased 46.1% as a result of 290 thermal applications performed and applied only in researches.

Longbiao [24] investigated the interface damage such as tensile and fracture on the thermal fatigue strength of ceramic-matrix composites (CMCs), which are fiber-reinforced composites. After thermal fatigue loading, the tensile and tensile strength and behaviors were investigated, and even fiber breakdowns were mentioned. The effect of thermal fatigue temperature, the main aspects affected by the number of cycles applied, internal damage, and tensile damage occurrences of the material were recorded and evaluated. The effects of clean CMCs under the influence of thermal fatigue loading, stress, fracture damage, thermal fatigue effects of temperature, thermal cycle number, fiber volume and area of use, interface shear initiative, fiber strength, and fiber Weibull module were evaluated together.

Mchale and Weaver [25] studied the morphing technology used to increase regeneration and multi-purpose use. Light, simple, convenient, and reliable works are always intended for industrial purposes. Composite materials are also open to using due to their light, suitable and durable usefulness. is worried. It greatly expands the design space to include antisymmetric and non-symmetric array arrays while improving the predictions of existing analytical models compared to experiments. The updated analytical model is presented and clarified using both finite element

models and experiments. While maintaining the stability of the products, research has been conducted with the aim of changes and innovations in thermal behavior.

Ghasemi et al. [26] examined the effects on structures with glass fiber reinforced polymer (GFRP) composite materials to investigate the thermal effects on composites, and to examine the thermal fatigue of different arrayed materials, and even to experimentally observe the interactions of multi-walled carbon nanotubes. By using the slitting method, it was desired to measure the thickness values. Also, an extended finite element analysis system was used to simulate the slicing process. During the examination of the experimental results, the effects of the change in thermal fatigue value on the composites were observed. The inversely proportional change of thermal residual stress with the number of thermal cycles was recorded. Finally, it has been found that symmetrical layout arrangements show less residual stress than non-symmetrical ones.

Second harmonic Lamb waves and thermal fatigue phenomenon in composites was examined by Li et al. [27]. Thermal cyclic loads are thought to undergo changes and wear for composite materials. The materials used in space and aircraft installation stages see that the minimal errors that occur create huge problems in the long run. To examine this phenomenon, it was aimed to develop non-destructive approaches. Minimal microscopic damage to linearity has proven to be a promising tool for early detection of micro damage after ultrasonic technical examinations. The present results wanted to evaluate and record a nonlinear monotonic increase with thermal fatigue cycles. The experimental observation between acoustic nonlinearity and thermal fatigue cycles in carbon/epoxy laminates proved that nonlinear Lamb waves can be used to study thermal fatigue damage, and it was aimed to draw the intended conclusions under the familiar linear-based assessment technique.

Li et al. [28] studied the theoretical and strengths that should be taken into consideration in the design of surface composites and design applications. Also, it has been aimed to examine the studies following high thermal fatigue performance by producing steel material surface composites reinforced and WC particles with vacuum steam formation mold casting. Also, the thermal fatigue coefficient of WC particles in composites was aimed to be produced and examined using a stereomicroscope, X-ray refraction, and scanning electron microscope. The effects of the composite material supported by WC particles in thermal fatigue failure and oxidation combinations during high-temperature formation were investigated. At a

temperature of approximately 500 degrees, if the thermal shock temperature is considered low, thermal fatigue failure at this temperature has degraded. However, oxidation particles were recorded by noticing their effects on thermal shock temperature. As a result, the particles to be described have shown their effect on thermal fatigue failures, including thermal strength.

Li et al. [29] investigated the thin laminate composites exposed to extreme humidity and temperature changes. Two factors that are predicted to be the reasons for the deterioration tendency and breakage in the materials are seen as extreme temperature change and high humidity. It has been desired to investigate the occurrence of the degradation development of composite laminates. The onset of deterioration and decay in unidirectional carbon/epoxy composite laminates, which are affected by humidity and high-temperature value, was characterized by Lamb waves and investigated through the records. The results show that thermal cyclic loading and moisture diffusion are two different conditions for the gradual degradation of composites under the bonding effect.

Pieniak et al. [30] investigated the fatigue formation in composites, the strength and thermal strength of polymer ceramic composites. The defining factors for these investigations are the development of mechanical strength, elastic modulus, and fracture development. With the effect of natural events and environmental factors, thermal fatigue was used and analyzed with a special computer-controlled device that performs thermal cycling algorithms. The composite materials created were applied as a thermal visor, each applied 104 times. Before the thermal cycle was started, the special design was immersed in the liquid and processed after a certain period of time. The elastic modulus of compositing used in the experiment was higher than that of the commercially specified composite (42%), it was found that the elastic modulus increased as the thermal loop increased. A descriptor known as the stress-fracture study, a device has been added to calculate the hydro-thermal fatigue of the polymer-ceramic composites tested.

Ghasemi et al. [31] examined the properties of the cured structure of nano-composite laminates. It is aimed to be examined by taking into account that stress values have a very high effect on engineering structures. The weight change was also examined together with the curvature strength. Also, it was aimed to keep the effects of thermal fatigue in mind and the results were given by examining every detail. Experimental results have shown that the addition of multi-walled carbon nanotubes (MWCNTs)

can cause different reactions in various epoxy resins, and the effects of nanoparticle addition vary greatly depending on the resin type and curing conditions. It was recorded that the lamina tendency is a variable due to thermal events.

Wu and Han [32] examined to perform numerical and analytical studies by defining the thermal fatigue behavior formation, crack propagation, and fracture surface properties of the SiCp / Al composite product added as melted (65% SiCp) produced by Pressure Infiltration Method. After the V notch formed on the composite was applied rotationally by thermal (300 degrees) heat treatment for 15 times and quenched with water, crack formation was observed at the tip of the notch. After examining the cracked surface with the necessary equipment, it has been determined that the formation of thermal fatigue cracks can increase the duration and duration of the fracture and even the crack will spread more easily. Finally, it has been found that reducing the size of the Reinforcing particles will increase the resistance of this type of composite material to thermal fatigue.

Zheng et al. [33] investigated Sialon - Si3N4 class composite ceramic materials examined by were produced by the pressing method. To be able to apply the thermal shock effect and thermal fatigue processes to ceramic composites, a water quenching process has been applied. The strength carcasses, as well as the resistance stance formed in the microstructure and their thermal behavior, were examined. According to the results, it has been observed that compared to the material in the ceramic structure, it exhibits higher bending strength kept under all thermal shock temperature differences, and accordingly, the product in the ceramic structure has higher strength. 600 degrees is accepted as the critical temperature. The crack growth of graded ceramic materials developed inversely with that of homogeneous ceramic materials and was lower. It was also found that the thermal shock effect was less. The fact that the properties have not changed much mechanically means that they maintain their stability.

Prakash [34] studied Caryota urens fibers combined with an acid, base, and silane were used during the production of products called epoxy biocomposite. The research aims to develop the production with this method and to reveal the characteristics of the development of Caryota fiber epoxy composite formation and its resistance to thermal events. The products were processed for 48 hours by applying the curing process. During the application of tensile bending tests, many mechanical properties were revealed. The fatigue behavior of the Caryota urens

epoxy composite recorded the highest fatigue life of 18,315 for 25% of the maximum stress tendency. SEM micrographs were found to be more useful and sticky for silane-treated CUF than previously applied acid and base. This product can be used in the defense industry, home appliances, and building formations to increase mechanical properties.

Schobel's [35] worked to be recorded as a good heat absorbent material for high power electronics, using a product intended for reinforcement using 60 percent diamond. Internal stresses due to temperature difference, stress evolution, during the thermal cycle between room temperature and 350 C the neutron breakage event has been studied one by one and shown in the graphs. Stress evolution has been demonstrated using high-resolution synchrotron tomography, with visco-plastic deformation of the Al matrix causing changes in void volume fraction and separation of the interface bond, even as thermal fatigue damage. The results were obtained in temperature formation.

Bahramian et al. [36] studied the materials exposed after the formation of aerodynamic heat in the earth's atmosphere were tried to be examined. Aircraft structures, spacecraft, even many composite structures that were processed ballistically can be damaged by the effect of severe aerodynamic heat. maybe the production and testing of the appropriate structure. Investigations can be made with special techniques and devices to prevent gravity. This study aims to model the ablation, combustion, and thermal degradation behavior of the heat shield resol-type phenolic resin/asbestos fabric composite in the oxyacetylene flame test and to present its technical properties. To calculate the heat transfer numerically, (FDM) method can be used. Analyzes were made with the ablation technique. It was observed that there was a change in the heat dissipation rate with thickness. Material design and thickness are very important factors in the calculation analysis of thermal protection shields.

Bellenger et al. [37] investigated the viscoelastic product formations are excellent structures that can dissipate some of the mechanical effects with heat due to environmental factors. While the point of dissipating heat is quite high in mechanical fatigue tests, they can provide heat dissipation until breaking, as stated. Even if the glass transition temperature of the PA66 matrix is not far from the ambient temperature, physical and mechanical changes do not take much time. For this reason, the graphs of the change of the temperature and the change of the material

are very detailed. During the test application, detailed numerical results were obtained with infrared devices. For a frequency of 10 Hz and although the test temperature is 23 ° C, the sample temperature on the surface is much higher. When examined with scanning electron microscopy, how and where the density error occurred was detailed.

Chen et al. [38] worked the natural aluminum matrix composite was formed by using 50% Si C particles (Al / SiCp) during the thermal cycling formed in composite materials and the formation of the plastic strain coefficient was investigated on the thermal expansion coefficient (CTE). The composite was produced with AL particles added as a liquid. The mechanical analysis of the composite and the evaluation of the thermal fatigue formation showed that the relationship between the CTE of Al / SiCp and temperature did not change linearly. The observations and investigations were taken when the CTE approached a maximum value. The theoretically accumulated plastic strain of Al / SiCp composites was also calculated by special formulation during thermal cycling formation and indicated on the graphs together with the experimental results.

Fei et al. [39] investigated the cooling processes of pure aluminum composite with SiC whisker added at high temperatures and its thermal resistance was compared from the maximum value to the minimum value. It was observed that sand formation in the material increased as the rate of thermal change increased. When the quenching with water started, using the transmission electron microscope and additionally checking the X-ray diffraction values, it was observed that the slow-cooled material dislocation density and thermal incompatibility (TMS) were lower than the fast-cooled composite. In addition to the results, it was recorded that the thermal expansion coefficient (CTE) was close to the rate of change of TMS and the dislocation density of the composite matrix. The TMS and CTE used during the study were noted with graphics and followed a good path for future studies.

Ferreira et al. [40] studied the fatigue state and properties of bonding structures by overlapping structures made of bi-directional woven e-glass fiber and polypropylene in some of the special production composite materials. The adhesive used is ethyl cyanoacrylate type known as special production. Research has been carried out on thermal and mechanical fatigue after overlapping of layer orientation. Results, curves formed after stress and the number of failure cycles are clearly defined and presented in the thesis. It has been added by specifying the damages in case of contact with

water. Fatigue damage and failure mechanisms are discussed while calculating numerically. It is thought that the dynamic hardness formation and thermal creep rates are the effects of fractures in the formation.

Giannadakis and Varna [41] examined the cracks that occur during the hardening events of the materials exposed to the peak temperatures and the thermal change cycles that are effective in the formation of laminate cracks. Some of the formations on fiber composite products also change mechanically and thermal. These effects on thermal and mechanical change are studied in this thesis.

Toudeshky and Mohammadi [42] examined the repairing aluminum composite materials with patches, repairing in one direction, applying repair in one direction, after the curing cycle following the stress conditions, the thermal efficiency. Specially arranged joints for cracks and taking into account the growth life of fatigue cracks were investigated. Curing procedures were aimed to be done carefully, considering the expansion sensitivity. (for example, 60 ° C). Also, FEM fatigue life and crack preforms obtained from the repaired panels were calculated by taking into account the thermal endurance lifetimes and it was verified to be in harmony.

Jeyaraj [43] investigated the numerical study on the vibration and acoustic properties of composite materials produced after cooling or quenching processes. Firstly, it was aimed to investigate the vibration analysis by taking into account the thermal conditions pre-stresses provided after the values determined following the critical temperatures. It is important for calculating the sound propagation after vibration calculation. Critical temperature and vibration were analyzed by finite element method based on Classical Laminate Sheet Theory (CLPT), and results were obtained with the combination of FEM / BEM sound radiation properties. The purpose of this research is to detail the effect of heat and the formation of cycles in the formation of micro-cracks.

Ju and Morgan [44] studied the composite specimens, radially fixing half-cylinders with two different sizes of product and two different stress factors. In the setup prepared by applying different temperature values, stress, the formation of thermal cycles, the effects of the heating or cooling rate, and its changes according to the humidity in the environment were observed. The results clearly showed us the effect of the number of thermal sheets, the effect of the created load factor, and the effect of the humidity in the environment on the material. Moreover, it was stated that the

most important reason for the interface slip was load adaptation under high temperatures. The resulting stresses caused the composite matrix to micro-crack.

Tubiana et al. [45] investigated the internal stresses of composite metal matrix products with an Al / SiCp addition. The elastoplastic deformations that occur after different heat treatments were recorded. An Eshelby type model was deemed appropriate to examine stress and different formations. The results of the experiment were compared with the model estimates obtained using an elastoplastic deformation model. Hydrostatic phase stresses occurring after heat treatment has been experimentally found. The plastic deformation that occurred changed and enabled micro-stressing processes to be clearly recorded.

Mehrman et al. [46] worked the fatigue behavior of an oxide-oxide ceramic-containing composite material has been investigated between the thermal change conditions and taking into account the ambient pressure and steam power. The stress formation caused by the laboratory air and steam effect is detailed. During the loading tests, calculations were made taking into account all the loads to which the material was exposed. The formation of steam in the environment significantly reduced the stress of the material performance. The lifetimes produced in the fatigue tests, the composite microstructure, and the damage and failure mechanisms were investigated.

Nousiainen et al. [47] investigation the PCSB composite connection structure and its thermal fatigue strength in low-temperature co-firing ceramic (LTCC) production were investigated. In the applied test, intergranular cracking and mixed intergranular cracking test mechanisms, the failure mechanism occurred at the outer edge of the connections, separation of the interface, and even cracking were observed. SAC-In soldered composite joints, which have a thermal fatigue event 75% longer than SAC composite joints have a perfect thermal strength coefficient under the specified conditions.

Petit et al. [48] examined the result of impact and compression (CAI) test values created after a composite laminate product coated with a cork thermal shield (TS) applied for coating formation. It was aimed to examine the differences of TS and non-TS materials and thermal and endurance strengths were calculated. The results show that TS provides mechanical protection against load build-up and even good exposure to the material. Additionally, different damage morphology between impact

testis with or without TS is presented in graphs. I would like to state that the TS coating is always stronger, especially at high impact energy.

Ray et al. [49] worked the fiber-reinforced composite materials containing polyester and epoxy resins are produced by keeping them at certain temperatures at certain intervals with different durations and it is aimed to be examined by being subjected to thermal shock. It was intended to evaluate the value of its strength during the 3-point bending test to observe the formation of inter-lamellar slip. Damage and fracture in some cases in bending tests where incompatibility occurs formation was observed. In the setup, it has foreseen to examine the mechanical factor of thermal shock-thermal fatigue.

Shariyat et al. [50] investigated the properties of rectangular and multi-layer composite materials, theoretical results were obtained by conducting thermal buckling experiments on a single type of temperature. It was supported by an experimental setup called Von Karman displacement or deformation. The equations were not simplified with the specified management. Although it is believed that the material properties change with temperature, Hermitian finite element formulation was created and the results are presented with data. The formulations were used during the displacement slip formations and even the force or moment limits were approximated. A FEM algorithm was created by specifying the boundary conditions clearly.

Shimokawa et al. [51] studied the effect of heat generated on composite materials. He discussed the cumulative frequency of micro cracks and the causes of crack formation of polymer-matrix composite materials at high temperature and the temperature factor in the progress of the formation. The experiment was started with a fixed application and the environment was not changed. Horizontal micro-cracks formed on the cross-sectional surface of the laminates during the programmed thermal cycle formation were recorded and plotted. stated that the cracking initial values and certain temperature values provide point changes. Si Tingzhi et al. [52] investigated the thermal shock fatigue phases formed on pure hot press alumina and analyzed the response of 30% TiC / Al2O3 composite materials by volume. Researches were conducted on the mechanical, thermal, and energy strengths of the first particle size composites of TiC and Al2O3. The research was conducted to evaluate the effect of the indentation-quenching test, thermal fatigue temperature value change, and thermal cycling formation on fatigue crack propagation. The effect

of monolithic alumina and TiC / Al2O3 composites on thermal shock fatigue are indicated as thermal fatigue and the main causes of thermal fatigue resistance of composites are indicated by the results of crack deflection.

Sobczak et al. [53] examined the short aluminum fibers, graphite, silicon carbide and fly ash particles. It is aimed to observe micro-cracks that occur during the formation of thermal cycles. Water quenching was applied after each thermal cycle. It was observed that the micro-crack structures changed in direct proportion to the number of thermal cycles. Among the materials used, those with high strength have been identified and recorded. The values taken as a basis in the experiment created were compared with the actual results and presented in the thesis.

2.3 Conclusions on Literature Survey

Literature on thermal fatigue was given in this chapter. Some problem about application of thermal fatigue failure method is noticed after reviewing these articles. Studies on thermal fatigue have started many years ago and these studies are still continuing today. In some studies, experimental setups have been formed, and in some studies thermal fatigue effects have been calculated over software programs. At the end of the experiments, the fatigue life of the materials was determined and it was observed how the materials behave under the cyclic temperatures.

In this thesis, thermal fatigue behavior of materials was investigated under the cyclic thermal loads. An algorithm developed under ANSYS finite element analysis software to determine the behavior of structures that are exposed repeated thermal loads by Yeter [1, 2] was adapted to the fiber reinforced composites.

CHAPTER 3

MATERIAL AND METHODS

3.1 Introduction

Methods and used algorithm to find thermal fatigue characteristics of materials are given in this chapter. Definition and main idea of fatigue and thermal fatigue are given firstly. Second, thermal fatigue algorithm and its details are discussed. Then, the used cases are given in this chapter.

3.2 Fatigue and Thermal Fatigue

3.2.1 Fatigue

Fatigue can be defined as the repeated loads that are applied to the structures in a random or systematic cycles. Wohler first defined the relation between applied stresses and cycles. This curve is generally called as (S-N) curve. Two main approach is proposed about the behavior of fatigue and they are Stress-life approach and strain-life approach, respectively. In the stress-life approach, the experiments are performed to get the cycle at which failure will start at a constant stress value. Then, by changing the stress value, the cycle at which failure will occur will be obtained and the S-N curve can be obtained. The main application types of fatigue are reversed type, fluctuating, and repeated type and they are given in the Figure 3.1.

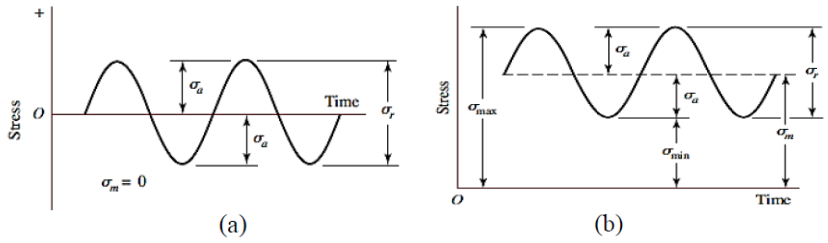

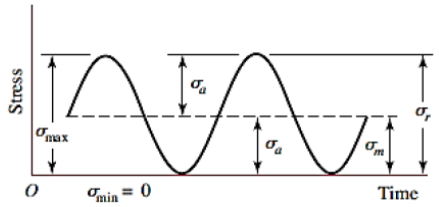

(c)

Figure 3.1 Stress-time curves. (a) Reversed type stress (b) Fluctuating stress

(c)Repeated type stress**.**

Fatigue design [55] is performed in areas exposed to stresses. In fatigue design problems, design is started by deciding the type of analysis first. Design for fatigue can be done either for infinite or finite life. If infinite life is chosen, the endurance limit is used. If finite life is chosen, fatigue strength is used during analyses.

Soderberg, Gerber and Goodman are generally used theories to design fatigue strength. Each theory has different formulations for fatigue design and these theories and formulations are listed in Table 3.1.

Table 3.1. Failure theories

	Formulation for safety factor (n)	
Theories	**Infinite life**	**Finite life**
Soderberg	$n = \frac{1}{\frac{Sa}{Se}+\frac{Sm}{Sy}}$	$n = \frac{1}{\frac{Sa}{Sf}+\frac{Sm}{Sy}}$
Gerber	$n = \frac{1}{\frac{Sa}{Se}+\frac{Sm^2}{Sut}}$	$n = \frac{1}{\frac{Sa}{Sf}+\frac{Sm^2}{Sut}}$
Goodman	$n = \frac{1}{\frac{Sa}{Se}+\frac{Sm}{Sut}}$	$n = \frac{1}{\frac{Sa}{Sf}+\frac{Sm}{Sut}}$
Where; S_a=Alternating Stress, S_m=Mean stress, S_e=endurance strength,		

S_{ut}= Ultimate stress,

3.2.3 Thermal Fatigue

Thermal fatigue [56] is the gradual deterioration and eventual cracking of a material by alternate heating and cooling during which free thermal expansion is partially or completely constrained. Thermal fatigue is a fatigue deficiency caused by cyclic thermal stresses and strains due to high temperature changes. Thermal fatigue may occur without mechanical loads. Compression stresses can be produced in a material with a high coefficient of thermal expansion. Tensile stresses can be produced in a material with a low coefficient of thermal expansion or generated when the material cools. When temperature changes, thermal stresses are generated by material expansion cyclical and contraction. Sometimes a crack may occur after many cyclic heating and cooling operations. In fact, the ductility of the material rather than the strength of the material determine the thermal fatigue life. Thermal fatigue can be divided into two, according to the magnitude of the thermal stress and the yield strength of the material; High Cycle Fatigue (HCF) or Low Cycle Fatigue (LCF). Thermal fatigue life can estimated the based on stress or plastic stress.

3.3 Thermal Fatigue Algorithm

In this thesis, the algorithm previously created by Yeter [1,2] has been adapted on composite materials. The flow chart used in this algorithm is given in Figure 3.2. Factor of safety can be determined via this algorithm.

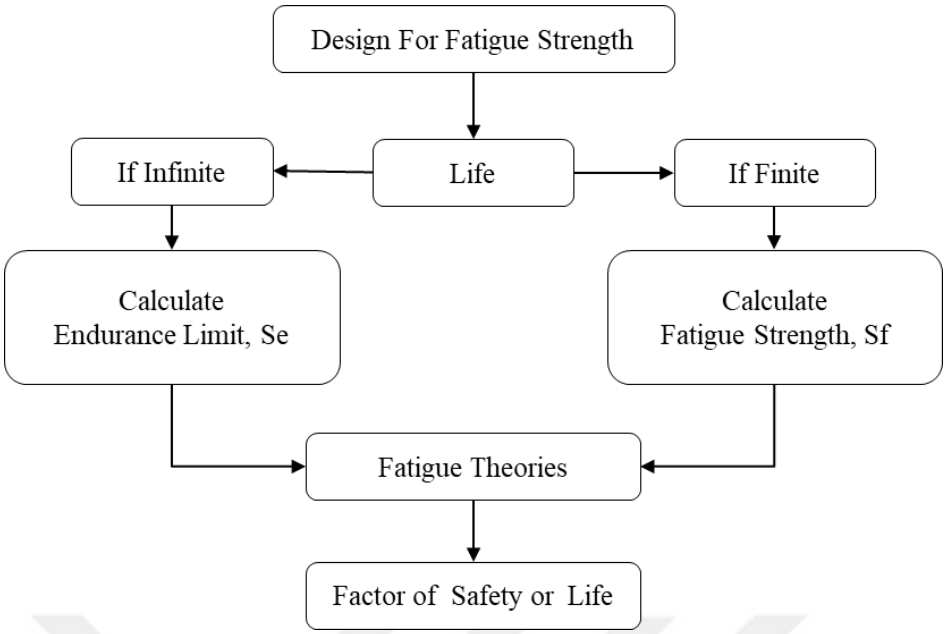

Figure 3.2 Flowchart for design for fatigue strength

To adapt the behavior of the composite material (layered laminate) to the algorithm, firstly the stress values are needed to the use in the safety factor value calculation using fatigue failure theorem. So the effects of thermal loads firstly needed to understand. For a laminate stress strain relation with thermal load starts to written strain for a lamina;

$$\begin{bmatrix} \varepsilon \\ \varepsilon \\ \gamma_{12} \end{bmatrix} = \begin{bmatrix} S_{11} & S_{12} & 0 \\ S_{12} & S_{22} & 0 \\ 0 & 0 & S_{66} \end{bmatrix} \begin{bmatrix} \sigma_1 \\ \sigma_2 \\ \tau_{12} \end{bmatrix} + \begin{bmatrix} {\varepsilon_1}^T \\ {\varepsilon_2}^T \\ 0 \end{bmatrix} \tag{3.1}$$

Where; the subscripts T is used to denote temperature.

The thermally induced strains are obtained by using equation (3.2).

$$\begin{bmatrix} {\varepsilon_1}^T \\ {\varepsilon_2}^T \\ 0 \end{bmatrix} = \Delta T \begin{bmatrix} \alpha_1 \\ \alpha_2 \\ 0 \end{bmatrix} \tag{3.2}$$

where α_1 and α_2 are the longitudinal and transverse coefficients of thermal expansion, respectively, and ΔT is the temperature change.

Equation (3.1) can be rearranged to get stress with equation (3.3).

$$\begin{bmatrix} \sigma_1 \\ \sigma_2 \\ \tau_{12} \end{bmatrix} = \begin{bmatrix} Q_{11} & Q_{12} & 0 \\ Q_{12} & Q_{22} & 0 \\ 0 & 0 & Q_{66} \end{bmatrix} \begin{bmatrix} \varepsilon_1 - {\varepsilon_1}^T \\ \varepsilon_2 - {\varepsilon_2}^T \\ \gamma_{12} \end{bmatrix} \tag{3.3}$$

The stress–strain relationship for an angle lamina is given in the equation 3.4.

$$\begin{bmatrix}\varepsilon_x\\ \varepsilon_y\\ \gamma_{xy}\end{bmatrix}=\begin{bmatrix}\overline{S}_{11} & \overline{S}_{12} & \overline{S}_{16}\\ \overline{S}_{12} & \overline{S}_{22} & \overline{S}_{26}\\ \overline{S}_{16} & \overline{S}_{26} & \overline{S}_{66}\end{bmatrix}\begin{bmatrix}\sigma_x\\ \sigma_y\\ \tau_{xy}\end{bmatrix}+\begin{bmatrix}{\varepsilon_x}^T\\ {\varepsilon_y}^T\\ {\gamma_{xy}}^T\end{bmatrix} \tag{3.4}$$

where:

$$\begin{bmatrix}{\varepsilon_x}^T\\ {\varepsilon_y}^T\\ {\gamma_{xy}}^T\end{bmatrix}=\Delta T\begin{bmatrix}\alpha_x\\ \alpha_y\\ \alpha_{xy}\end{bmatrix} \tag{3.5}$$

The terms α_x, α_y, and α_{xy} are the coefficients of thermal expansion for an angle lamina and are given in terms of the coefficients of thermal expansion for a unidirectional lamina as:

$$\begin{bmatrix}\alpha_x\\ \alpha_y\\ \alpha_{xy}\end{bmatrix}=\lfloor T\rfloor^{-1}\begin{bmatrix}\alpha_1\\ \alpha_2\\ 0\end{bmatrix} \tag{3.6}$$

Excess of or less than the hydrothermal strains in the unrestricted lamina produce the residual stresses. These strain differences are called mechanical strains and the stresses caused by them are called mechanical stresses. These stresses are obtained using equation 3.7.

$$\begin{bmatrix}{\varepsilon_x}^M\\ {\varepsilon_y}^M\\ {\gamma_{xy}}^M\end{bmatrix}_l=\begin{bmatrix}\varepsilon_x\\ \varepsilon_y\\ \gamma_{xy}\end{bmatrix}_l-\begin{bmatrix}{\varepsilon_x}^T\\ {\varepsilon_y}^T\\ {\gamma_{xy}}^T\end{bmatrix}_l=\begin{bmatrix}\varepsilon_x\\ \varepsilon_y\\ \gamma_{xy}\end{bmatrix}_l-\begin{bmatrix}\alpha_x\Delta T\\ \alpha_y\Delta T\\ \alpha_{xy}\Delta T\end{bmatrix}_l \tag{3.7}$$

where the superscript *M* represents the mechanical strains, *T* stands for the free expansion thermal strain, and *l* refers to the layer.

Stress–strain relation for an angle-lamina can be obtained using the equation 3.8.

$$\begin{bmatrix}\sigma_x\\ \sigma_y\\ \tau_{xy}\end{bmatrix}=\begin{bmatrix}\overline{Q}_{11} & \overline{Q}_{12} & \overline{Q}_{16}\\ \overline{Q}_{12} & \overline{Q}_{22} & \overline{Q}_{26}\\ \overline{Q}_{16} & \overline{Q}_{26} & \overline{Q}_{66}\end{bmatrix}\begin{bmatrix}\varepsilon_x\\ \varepsilon_y\\ \gamma_{xy}\end{bmatrix} \tag{3.8}$$

Using stress–strain Equation (3.8), the hydrothermal stresses in a lamina are then given by;

$$\begin{bmatrix}{\sigma_x}^T\\ {\sigma_y}^T\\ {\tau_{xy}}^T\end{bmatrix}=\begin{bmatrix}\overline{Q}_{11} & \overline{Q}_{12} & \overline{Q}_{16}\\ \overline{Q}_{12} & \overline{Q}_{22} & \overline{Q}_{26}\\ \overline{Q}_{16} & \overline{Q}_{26} & \overline{Q}_{66}\end{bmatrix}\begin{bmatrix}{\varepsilon_x}^M\\ {\varepsilon_y}^M\\ {\gamma_{xy}}^M\end{bmatrix} \tag{3.9}$$

Hydrothermal stresses induce zero resultant forces and moments in the laminate. And the resultant force and moment equations for total laminate can be written as:

$$\int_{-h/2}^{+h/2} \begin{bmatrix} {\sigma_x}^T \\ {\sigma_y}^T \\ {\tau_{xy}}^T \end{bmatrix} dz = 0 \text{ and } \int_{-h/2}^{+h/2} \begin{bmatrix} {\sigma_x}^T \\ {\sigma_y}^T \\ {\tau_{xy}}^T \end{bmatrix} z dz = 0 \quad (3.10)$$

Also equation (3.10) can be written by integration for each layer and adding the result of each integration to get results of whole laminate using equation (3.11).

$$\sum_{k=1}^{n} \int_{hk-1}^{hk} \begin{bmatrix} {\sigma_x}^T \\ {\sigma_y}^T \\ {\tau_{xy}}^T \end{bmatrix} dz = 0 \text{ and } \sum_{k=1}^{n} \int_{hk-1}^{hk} \begin{bmatrix} {\sigma_x}^T \\ {\sigma_y}^T \\ {\tau_{xy}}^T \end{bmatrix} z\, dz = 0 \quad (3.12)$$

Putting Equation (3.9) to Equation (3.12);

$$\sum_{k=1}^{n} \int_{hk-1}^{hk} \begin{bmatrix} \overline{Q}_{11} & \overline{Q}_{12} & \overline{Q}_{16} \\ \overline{Q}_{12} & \overline{Q}_{22} & \overline{Q}_{26} \\ \overline{Q}_{16} & \overline{Q}_{26} & \overline{Q}_{66} \end{bmatrix} \begin{bmatrix} {\varepsilon_x}^M \\ {\varepsilon_y}^M \\ {\gamma_{xy}}^M \end{bmatrix} dz = 0 \quad (3.13)$$

and

$$\sum_{k=1}^{n} \int_{hk-1}^{hk} \begin{bmatrix} \overline{Q}_{11} & \overline{Q}_{12} & \overline{Q}_{16} \\ \overline{Q}_{12} & \overline{Q}_{22} & \overline{Q}_{26} \\ \overline{Q}_{16} & \overline{Q}_{26} & \overline{Q}_{66} \end{bmatrix} \begin{bmatrix} {\varepsilon_x}^M \\ {\varepsilon_y}^M \\ {\gamma_{xy}}^M \end{bmatrix} z dz = 0 \quad (3.14)$$

Substituting Equation (3.7) into the Equation (3.13) gives

$$\sum_{k=1}^{n} \int_{hk-1}^{hk} \begin{bmatrix} \overline{Q}_{11} & \overline{Q}_{12} & \overline{Q}_{16} \\ \overline{Q}_{12} & \overline{Q}_{22} & \overline{Q}_{26} \\ \overline{Q}_{16} & \overline{Q}_{26} & \overline{Q}_{66} \end{bmatrix} \left[\begin{bmatrix} \varepsilon_x \\ \varepsilon_y \\ \gamma_{xy} \end{bmatrix}_l - \begin{bmatrix} {\varepsilon_x}^T \\ {\varepsilon_y}^T \\ {\gamma_{xy}}^T \end{bmatrix}_l \right] dz = 0 \quad (3.15)$$

The strain equation can be written as given 3.15 using mid-plane strain and curvatures.

$$\begin{bmatrix} \varepsilon_x \\ \varepsilon_y \\ \gamma_{xy} \end{bmatrix} = \begin{bmatrix} {\varepsilon_x}^0 \\ {\varepsilon_y}^0 \\ {\gamma_{xy}}^0 \end{bmatrix} + z \begin{bmatrix} \kappa_x \\ \kappa_y \\ \kappa_{xy} \end{bmatrix} \quad (3.16)$$

Substituting Equation (3.16) into the equation (3.15) gives;

$$\sum_{k=1}^{n} \int_{hk-1}^{hk} \begin{bmatrix} \overline{Q}_{11} & \overline{Q}_{12} & \overline{Q}_{16} \\ \overline{Q}_{12} & \overline{Q}_{22} & \overline{Q}_{26} \\ \overline{Q}_{16} & \overline{Q}_{26} & \overline{Q}_{66} \end{bmatrix} \left[\begin{bmatrix} {\varepsilon_x}^0 \\ {\varepsilon_y}^0 \\ {\gamma_{xy}}^0 \end{bmatrix} + z \begin{bmatrix} \kappa_x \\ \kappa_y \\ \kappa_{xy} \end{bmatrix} - \begin{bmatrix} {\varepsilon_x}^T \\ {\varepsilon_y}^T \\ {\gamma_{xy}}^T \end{bmatrix}_l \right] dz = 0 \quad (3.17)$$

If the equation 3.17 is rearranged, then;

$$\sum_{k=1}^{n} \int_{hk-1}^{hk} \begin{bmatrix} \overline{Q}_{11} & \overline{Q}_{12} & \overline{Q}_{16} \\ \overline{Q}_{12} & \overline{Q}_{22} & \overline{Q}_{26} \\ \overline{Q}_{16} & \overline{Q}_{26} & \overline{Q}_{66} \end{bmatrix} \left(\begin{bmatrix} {\varepsilon_x}^0 \\ {\varepsilon_y}^0 \\ {\gamma_{xy}}^0 \end{bmatrix} + z \begin{bmatrix} \kappa_x \\ \kappa_y \\ \kappa_{xy} \end{bmatrix} \right) dz =$$

$$\sum_{k=1}^{n} \int_{hk-1}^{hk} \begin{bmatrix} \overline{Q}_{11} & \overline{Q}_{12} & \overline{Q}_{16} \\ \overline{Q}_{12} & \overline{Q}_{22} & \overline{Q}_{26} \\ \overline{Q}_{16} & \overline{Q}_{26} & \overline{Q}_{66} \end{bmatrix} \left(\begin{bmatrix} {\varepsilon_x}^T \\ {\varepsilon_y}^T \\ {\gamma_{xy}}^T \end{bmatrix}_l \right) dz \tag{3.18}$$

Substituting equation (3.5) into the right side of the equation (3.18) gives;

$$\sum_{k=1}^{n} \int_{hk-1}^{hk} \begin{bmatrix} \overline{Q}_{11} & \overline{Q}_{12} & \overline{Q}_{16} \\ \overline{Q}_{12} & \overline{Q}_{22} & \overline{Q}_{26} \\ \overline{Q}_{16} & \overline{Q}_{26} & \overline{Q}_{66} \end{bmatrix} \left(\begin{bmatrix} {\varepsilon_x}^0 \\ {\varepsilon_y}^0 \\ {\gamma_{xy}}^0 \end{bmatrix} + z \begin{bmatrix} \kappa_x \\ \kappa_y \\ \kappa_{xy} \end{bmatrix} \right) dz =$$

$$\sum_{k=1}^{n} \int_{hk-1}^{hk} \begin{bmatrix} \overline{Q}_{11} & \overline{Q}_{12} & \overline{Q}_{16} \\ \overline{Q}_{12} & \overline{Q}_{22} & \overline{Q}_{26} \\ \overline{Q}_{16} & \overline{Q}_{26} & \overline{Q}_{66} \end{bmatrix} \left(\begin{bmatrix} \alpha_x \\ \alpha_y \\ \alpha_{xy} \end{bmatrix}_l \Delta T \right) dz \tag{3.19}$$

Since the right side of the equation 3.19 is the general load and mid plane strain and curvatures equations, the equation 3.19 can be rewritten as;

$$\begin{bmatrix} A_{11} & A_{12} & A_{16} \\ A_{12} & A_{22} & A_{26} \\ A_{16} & A_{26} & A_{66} \end{bmatrix} \left(\begin{bmatrix} {\varepsilon_x}^0 \\ {\varepsilon_y}^0 \\ {\gamma_{xy}}^0 \end{bmatrix} + \begin{bmatrix} B_{11} & B_{12} & B_{16} \\ B_{12} & B_{22} & B_{26} \\ B_{16} & B_{26} & B_{66} \end{bmatrix} \begin{bmatrix} \kappa_x \\ \kappa_y \\ \kappa_{xy} \end{bmatrix} \right) = \begin{bmatrix} {N_x}^T \\ {N_y}^T \\ {N_{xy}}^T \end{bmatrix} \tag{3.20}$$

where;

$$\begin{bmatrix} {N_x}^T \\ {N_y}^T \\ {N_{xy}}^T \end{bmatrix} = \sum_{k=1}^{n} \int_{hk-1}^{hk} \begin{bmatrix} \overline{Q}_{11} & \overline{Q}_{12} & \overline{Q}_{16} \\ \overline{Q}_{12} & \overline{Q}_{22} & \overline{Q}_{26} \\ \overline{Q}_{16} & \overline{Q}_{26} & \overline{Q}_{66} \end{bmatrix} \left(\begin{bmatrix} \alpha_x \\ \alpha_y \\ \alpha_{xy} \end{bmatrix}_l \Delta T \right) dz =$$

$$\Delta T \sum_{l=1}^{n} \begin{bmatrix} \overline{Q}_{11} & \overline{Q}_{12} & \overline{Q}_{16} \\ \overline{Q}_{12} & \overline{Q}_{22} & \overline{Q}_{26} \\ \overline{Q}_{16} & \overline{Q}_{26} & \overline{Q}_{66} \end{bmatrix}_l \begin{bmatrix} \alpha_x \\ \alpha_y \\ \alpha_{xy} \end{bmatrix}_l (h_l - h_{l-1})$$

(3.21)

Also similar operations can be performed to the moment equation (3.14) and as a result equation (3.22) will be obtained.

$$\begin{bmatrix} B_{11} & B_{12} & B_{16} \\ B_{12} & B_{22} & B_{26} \\ B_{16} & B_{26} & B_{66} \end{bmatrix} \left[\begin{bmatrix} {\varepsilon_x}^0 \\ {\varepsilon_y}^0 \\ {\gamma_{xy}}^0 \end{bmatrix} + \begin{bmatrix} D_{11} & D_{12} & D_{16} \\ D_{12} & D_{22} & D_{26} \\ D_{16} & D_{26} & D_{66} \end{bmatrix} \begin{bmatrix} \kappa_x \\ \kappa_y \\ \kappa_{xy} \end{bmatrix} \right] = \begin{bmatrix} {M_x}^T \\ {M_y}^T \\ {M_{xy}}^T \end{bmatrix} \tag{3.22}$$

where;

$$\begin{bmatrix} {M_x}^T \\ {M_y}^T \\ {M_{xy}}^T \end{bmatrix} = \sum_{k=1}^{n} \int_{hk-1}^{hk} \begin{bmatrix} \overline{Q}_{11} & \overline{Q}_{12} & \overline{Q}_{16} \\ \overline{Q}_{12} & \overline{Q}_{22} & \overline{Q}_{26} \\ \overline{Q}_{16} & \overline{Q}_{26} & \overline{Q}_{66} \end{bmatrix} \left[\begin{bmatrix} \alpha_x \\ \alpha_y \\ \alpha_{xy} \end{bmatrix}_l \Delta T \right] z \, dz$$

$$= \frac{1}{2} \Delta T \sum_{l=1}^{n} \begin{bmatrix} \overline{Q}_{11} & \overline{Q}_{12} & \overline{Q}_{16} \\ \overline{Q}_{12} & \overline{Q}_{22} & \overline{Q}_{26} \\ \overline{Q}_{16} & \overline{Q}_{26} & \overline{Q}_{66} \end{bmatrix}_l \begin{bmatrix} \alpha_x \\ \alpha_y \\ \alpha_{xy} \end{bmatrix}_l ({h_l}^2 - {h_{l-1}}^2) \tag{3.23}$$

The loads in equation (3.21) to equation (3.23) are called fictitious thermal loads and are known (applied loads as a results of thermal loading). One can calculate the mid-plane strains and curvatures by combining equation (3.20) and equation (3.22):

$$\begin{bmatrix} {N_x}^T \\ {N_y}^T \\ {N_{xy}}^T \\ {M_x}^T \\ {M_y}^T \\ {M_{xy}}^T \end{bmatrix} = \begin{bmatrix} A_{11} & A_{12} & A_{16} & B_{11} & B_{12} & B_{16} \\ A_{12} & A_{22} & A_{26} & B_{12} & B_{22} & B_{26} \\ A_{16} & A_{26} & A_{66} & B_{16} & B_{26} & B_{66} \\ B_{11} & B_{12} & B_{16} & D_{11} & D_{12} & D_{16} \\ B_{12} & B_{22} & B_{26} & D_{12} & D_{22} & D_{26} \\ B_{16} & B_{26} & B_{66} & D_{16} & D_{26} & D_{66} \end{bmatrix} \begin{bmatrix} {\varepsilon_x}^0 \\ {\varepsilon_y}^0 \\ {\varepsilon_{xy}}^0 \\ \kappa_x \\ \kappa_y \\ \kappa_{xy} \end{bmatrix} \tag{3.24}$$

where; [A] is the extensional stiffness matrix which is the resultant in-plane loads to the in-plane strains. [B] is the coupling stiffness matrix coupling the load and moments with the mid-plane strains and curvatures. [D] is bending stiffness matrix which is the resultant bending moments to the plate curvatures.

By solving the equation 3.24, the mid-plane strains and curvatures can be obtained. Then, global strains in any ply of the laminate can be calculated the using eq. (3.16).

Also the global stress values can be obtained using the equation 3.8. Average stress values for total laminate are considered in the algorithm that is adapted to the composite plates. Stress results of each layer are obtained from in mid-plane. In order to inspect the thermal stresses of the plates, the SHELL181 element type is used. SHELL181 [57] can be used for layered applications for modeling composite shells or sandwich construction. The accuracy in modeling composite shells is governed by the first-order shear-deformation theory. After obtaining the stress values after thermal loading the alternating and mean stresses are obtained using these values and following equations (3.25-3.31).

$$Sa_x = \frac{\sigma_{x2} - \sigma_{x1}}{2} \tag{3.25}$$

$$Sa_y = \frac{\sigma_{y2} - \sigma_{y1}}{2} \tag{3.26}$$

$$Sa_{xz} = \frac{\sigma_{xz2} - \sigma_{xz1}}{2} \tag{3.27}$$

$$Sa_{xy} = \frac{\sigma_{xy2} - \sigma_{xy1}}{2} \tag{3.28}$$

$$Sm_x = \frac{\sigma_{x2} - \sigma_{x1}}{2}$$

$$Sm_{xy} = \frac{\sigma_{xy2} - \sigma_{xy1}}{2} \tag{3.29}$$

$$Sm_y = \frac{\sigma_{y2} - \sigma_{y1}}{2} \tag{3.30}$$

$$Sm_{xz} = \frac{\sigma_{xz2} - \sigma_{xz1}}{2} \tag{3.31}$$

$$S_a = \sqrt{\frac{1}{2}\left[\left(Sa_x - Sa_y\right)^2 + (Sa_x - Sa_z)^2 + \left(Sa_z - Sa_y\right)^2\right] + 3\left(Sa_{xy}{}^2 + Sa_{xz}{}^2 + Sa_{yz}{}^2\right)} \tag{3.32}$$

$$S_m = \sqrt{\frac{1}{2}\left[\left(Sm_x - Sm_y\right)^2 + (Sm_x - Sm_z)^2 + \left(Sm_z - Sm_y\right)^2\right] + 3\left(Sm_{xy}{}^2 + Sm_{xz}{}^2 + Sm_{yz}{}^2\right)} \tag{3.33}$$

$$S_e = k_a k_b k_c k_d k_e k_f S_e' \tag{3.34}$$

$$S_e' = \begin{cases} 0.5\, S_{ut} & S_{ut} \leq 1400\ MPa \\ 700\ MPa & S_{ut} > 1400\ MPa \end{cases} \tag{3.35}$$

ka, kb, kc, kd, ke, kf taken as a 1. Then Safety factor (n) is calculated by using equation 3.36.

$$n = \frac{1}{\frac{S_a}{S_e} + \frac{S_m}{S_y}} \tag{3.36}$$

In this thesis, the uniform temperature was assigned to the nodes considering reference temperature as 25°C. Like a structural analysis under the mechanical loads, the thermal strains are obtained after each load cycle. Surface of the element can be subjected to both maximum tension and maximum compression stresses in one full rotation. Firstly, +100°C uniform temperature load was applied and then the plate subjected to -130°C thermal load. Thermal strains are obtained for both types of loadings. The safety factor distributions of plates were predicted using the failure criteria, obtained stresses from thermal strains, and the other material properties. The material properties of the used composite laminates are given in Table 3.2. These material properties, determined in standard conditions (room-temperature), are taken from a textbook [58].

Table 3.2 Mechanical properties [58]

Property	Units	Glass/Epoxy	Boron/Epoxy	Graphite/Epoxy
Longitudinal elastic modulus (E1)	GPa	38.6	204	181
Transverse elastic modulus (E2)	GPa	8.27	18.50	10.30
Major Poisson's ratio (ν_{12})		0.26	0.23	0.28
Shear Modulus (G_{12})	GPa	4.14	5.59	7.17
Ultimate longitudinal tensile strength	MPa	1062	1260	1500
Ultimate longitudinal compressive strength	MPa	610	2500	1500
Ultimate transverse tensile strength	MPa	31	61	40
Ultimate transverse compressive strength	MPa	118	202	246
Ultimate in-plane shear strength	MPa	72	67	68

3.4 Case Studies

Different cases are used in this thesis. The used plate dimensions are taken as constant and these dimensions are 100 mm length, 50 mm width. Each layer thickness is taken as 0.25 mm. +100°C uniform temperature load was applied and then the plate subjected to -130°C thermal load. The reference temperature was taken as 25 C° in fatigue cycles. The boundary conditions given in Figure 3.3 are used. As seen in this figure, the all edges of the plate are fixed (fix-all), and left and right edge fixed (fix-fix) boundary conditions are considered. $[(0/90)_2]_s$, $[(15/-75)_2]_s$, $[(30/-60)_2]_s$, and $[(45/-45)_2]_s$ fiber orientation are used.

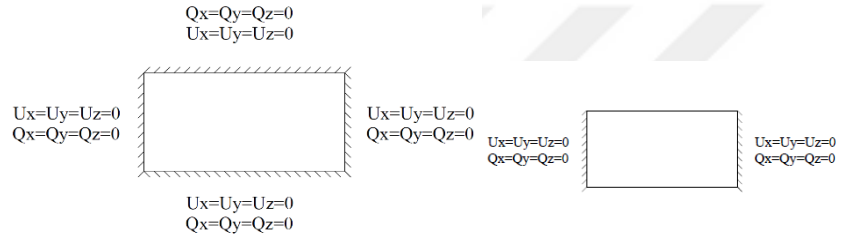

Figure 3.3 Two boundary condition, (a) fix-all and (b) fix-fix used.

Also, circular cutouts are used and +100°C and -130°C cyclic thermal loading is performed considering different materials. The reference temperature was taken as 25 C°. The boundary conditions and used cutouts are given in Figure 3.4 and Figure 3.5. As seen in this figures, the all edges of the plate are fixed (fix-all), and left and right edge fixed (fix-fix) boundary conditions are considered. During analyses, 5 different cut-out sizes are considered. For circular cut-out diameter (A) is taken as 10, 15, 20, 25, and 30 mm and 11 different cutout positions (CL) -25, -20, -15, -10, -5, 0, 5, 10, 15, 20, and 25 are used.

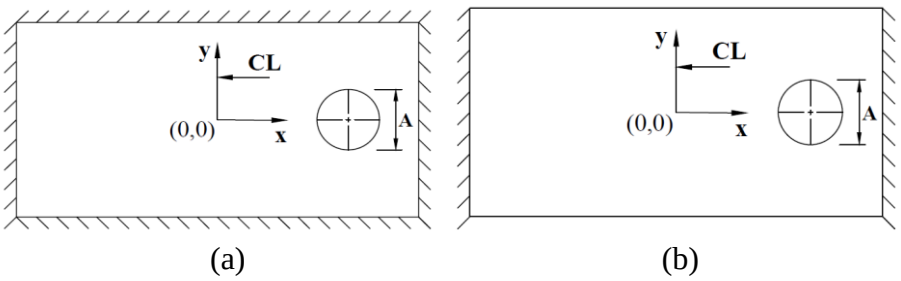

Figure 3.4 Boundary conditions with cut-outs (a) all-fix, (b) fix-fix

CHAPTER 4

RESULTS AND DISCUSSIONS

4.1 Introduction

Safety factor distributions of Glass/Epoxy, Graphite/Epoxy, and Boron/Epoxy fiber reinforced composites under the thermal fatigue loads are given in this chapter. The results are given with 2 main section and sub-sections. In section 4.2, results of thermal fatigue load for different fiber orientations $[(0/90)_2]_s$, $[(15/-75)_2]_s$, $[(30/-60)_2]_s$, and $[(45/-45)_2]_s$ are given. In this section result that shown effects of different fibers types and fiber orientation and ply stacking sequences are given. In section 4.3, results shown effects of cutouts and their positions on the thermal fatigue loads for composite materials are given.

4.2 Results for Thermal Fatigue behavior of composites

In this section, behavior of polymer matrix composites under the thermal fatigue loads are given considering pure thermal cyclic loads. Factor of safety distribution for fix-all boundary condition under pure thermal fatigue load for $[(0/90)_2]_s$ are compared for Glass/Epoxy, Graphite/Epoxy and Boron/Epoxy composites in Figure 4.1. The figure emphases that Graphite/Epoxy laminate has the highest factor of safety value and Boron/Epoxy has the minimum factor of safety value. As illustrated in Figure 4.3 for Glass/Epoxy, the safety factor values for fiber orientation angles are same. The safety factor results obtained for fix-fix boundary conditions are presented in figure 4.2 for Glass/Epoxy laminates for $[(0/90)_2]_s$, $[(15/-75)_2]_s$, $[(30/-60)_2]_s$, and $[(45/-45)_2]_s$ fiber orientations and ply sequences. Also Figure 4.3 presents the variation of the lowest factor of safety respect to different fiber orientations and ply sequences. As seen these figures, for fix-fix boundary conditions fiber orientations has direct effects on the safety factor value of laminates. $[(0/90)_2]_s$, ply sequence has the highest safety factor and $[(45/-45)_2]_s$ has the lowest safety factor value. The safety

factor values of $[(15/-75)_2]_s$, and $[(30/-60)_2]_s$ are between $[(0/90)_2]_s$ and $[(45/-45)_2]_s$ ply sequences.

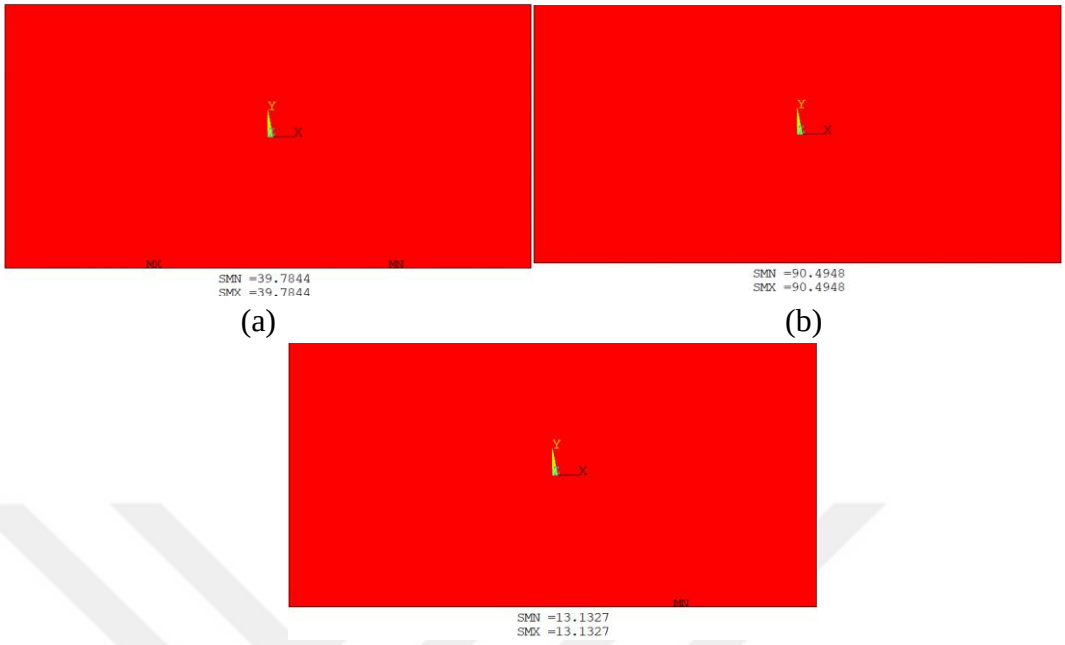

(a) (b)

(c)

Figure 4.1 Factor of safety for fix-all boundary condition under pure thermal fatigue for $[(0/90)_2]_s$ orientation (a) Glass/Epoxy, (b) Graphite/Epoxy (c) Boron/Epoxy

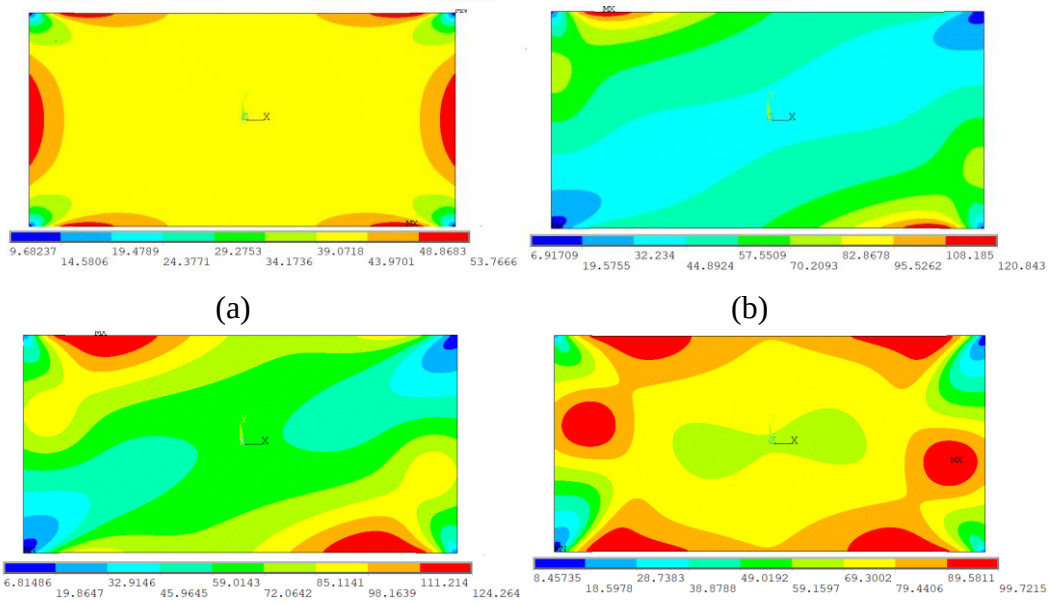

(a) (b)

(c) (d)

Figure 4.2 Safety factor distribution of Glass/Epoxy for fix-fix boundary condition at different fiber orientations (a) $[(0/90)_2]_s$, (b) $[(15/-75)_2]_s$, (c) $[(30/-60)_2]_s$, (d) $[(45/-45)_2]_s$

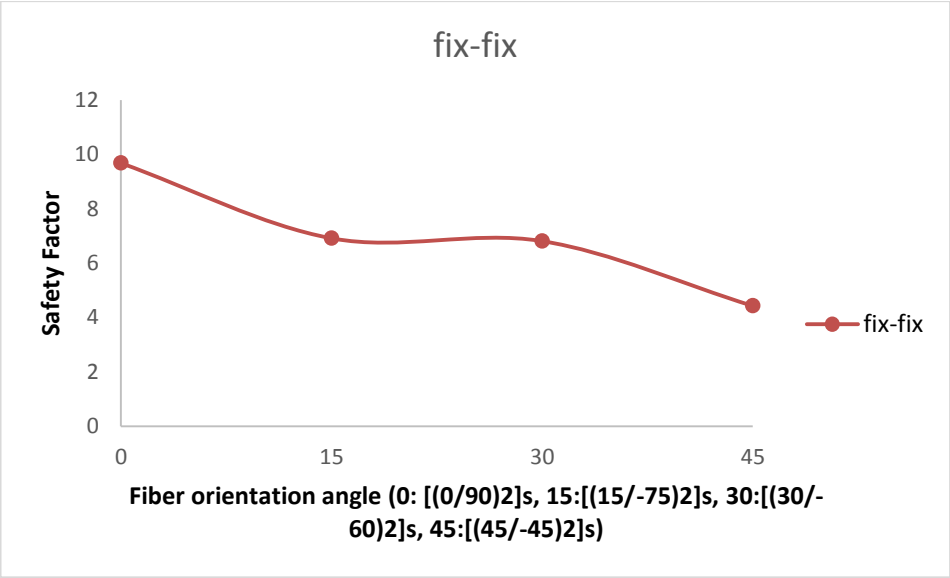

(a)

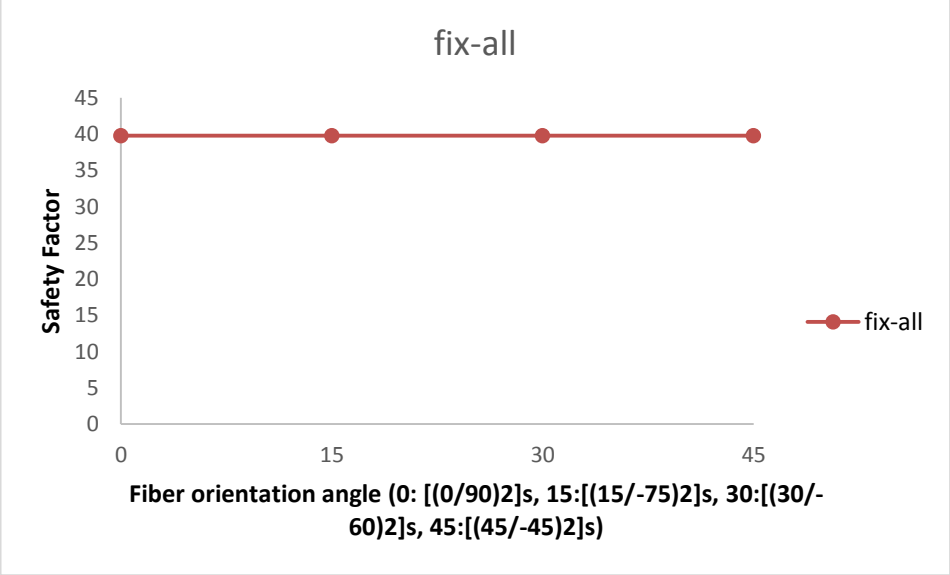

(b)

Figure 4.3 Variation of safety factor of Glass/Epoxy with Fiber orientation angle for different boundary conditions (a) Fix-Fix, (b) Fix-all

The safety factor results obtained for fix-fix boundary conditions are given in figure 4.4 for Graphite /Epoxy laminates for $[(0/90)_2]_s$, $[(15/-75)_2]_s$, $[(30/-60)_2]_s$, and $[(45/-45)_2]_s$ fiber orientations and ply sequences. Also Figure 4.4 presents the variation of the lowest factor of safety respect to different fiber orientations and ply sequences. For fix-fix boundary conditions and Graphite/Epoxy $[(0/90)_2]_s$, ply sequence has the highest safety factor value as the Graphite/Epoxy. When ply sequences changes to the $[(15/-75)_2]_s$ the safety factor value decreases. But after $[(30/-60)_2]_s$ ply sequences

the safety factor value is started to increase. For all-fix conditions each ply orientations have the same safety factor value.

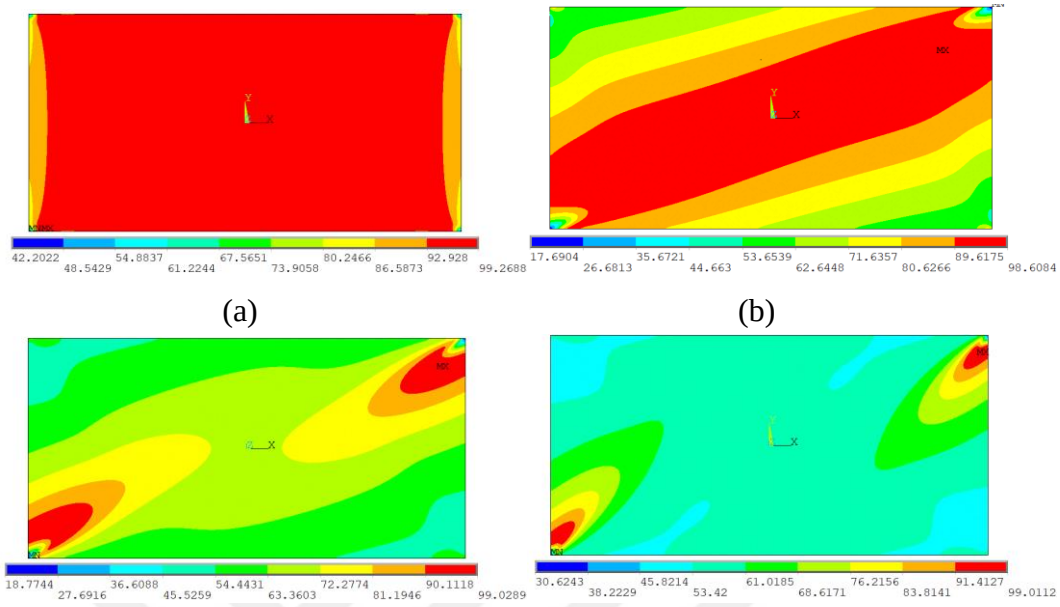

Figure 4.4 Safety factor distribution of Graphite/Epoxy for fix-fix boundary condition at different fiber orientations (a) $[(0/90)_2]_s$, (b) $[(15/-75)_2]_s$, (c) $[(30/-60)_2]_s$, (d) $[(45/-45)_2]_s$

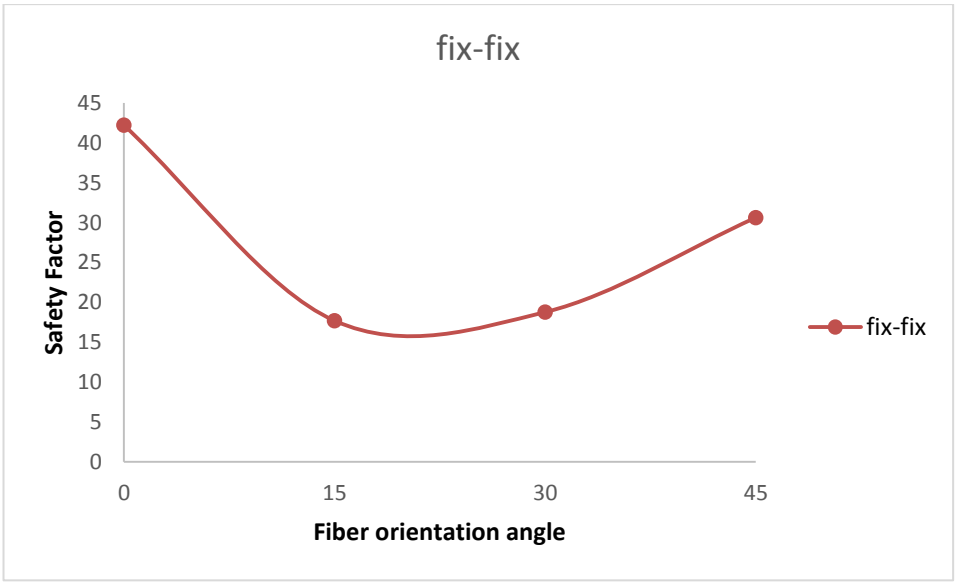

(a)

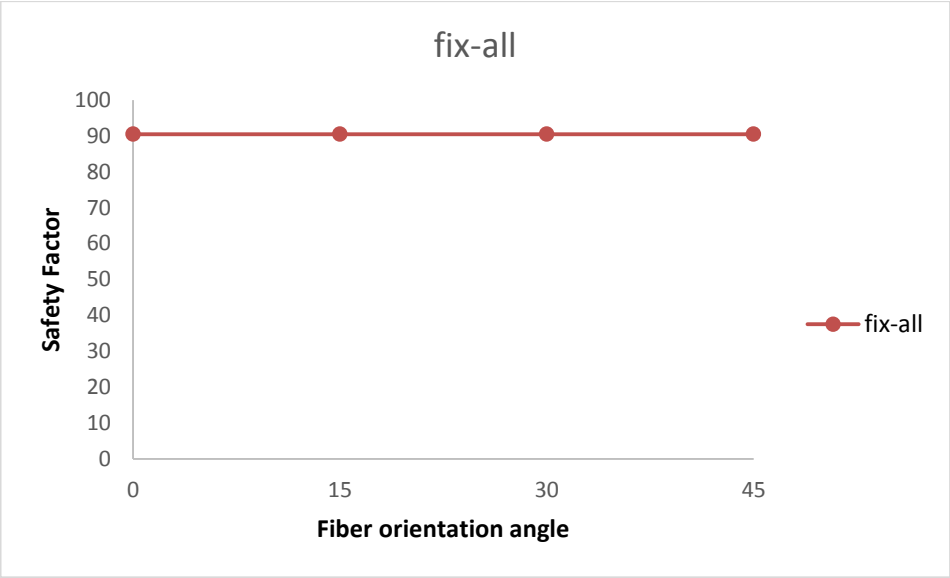

(b)

Figure 4.5 Variation of safety factor of Graphite/Epoxy with Fiber orientation angle for different boundary conditions (a) Fix-Fix, (b) Fix-all

The results obtained for fix-fix boundary conditions are given in figure 4.6 for Boron /Epoxy laminates for $[(0/90)_2]_s$, $[(15/-75)_2]_s$, $[(30/-60)_2]_s$, and $[(45/-45)_2]_s$ fiber orientations and ply sequences. Also Figure 4.6 presents the variation of the lowest factor of safety respect to different fiber orientations and ply sequences. As seen in these figures maximum minimum values are different but the behavior of safety factor variation is same.

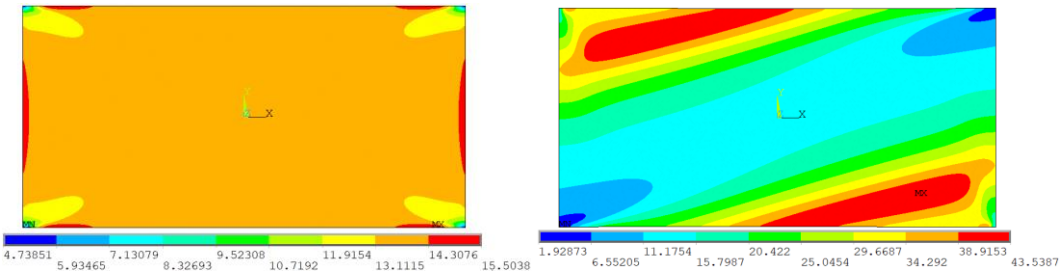

(a) (b)

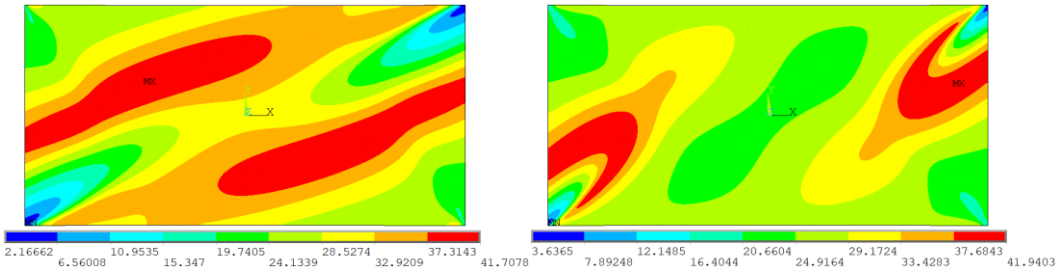

(c) (d)

Figure 4.6 Safety factor distribution of Boron/Epoxy for fix-fix boundary condition at different fiber orientations (a) $[(0/90)_2]_s$, (b) $[(15/-75)_2]_s$, (c) $[(30/-60)_2]_s$, (d) $[(45/-45)_2]_s$

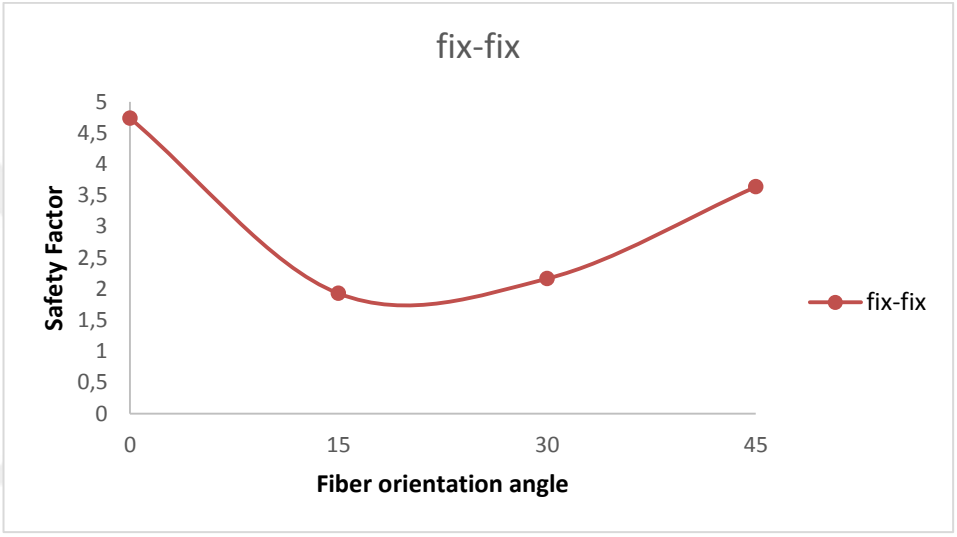

(a)

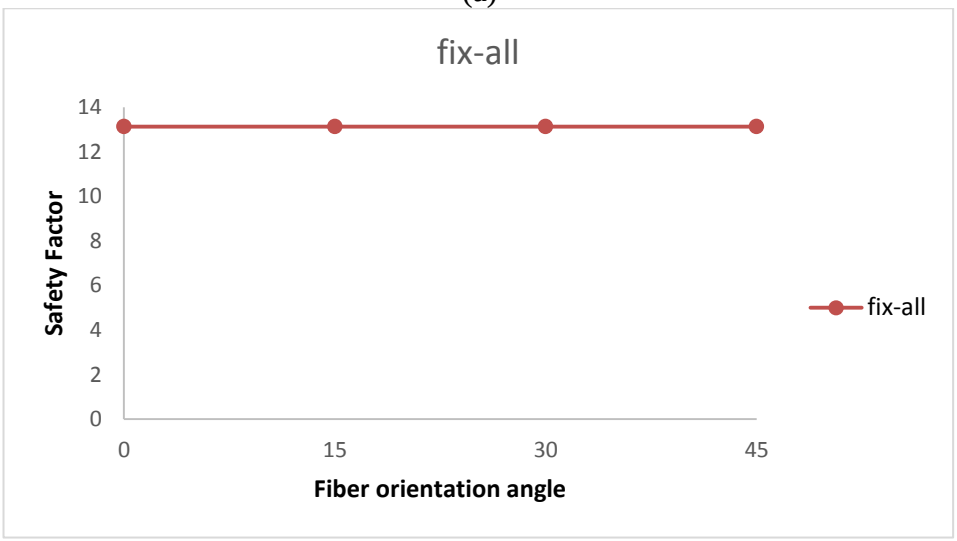

(b)

Figure 4.7 Variation of safety factor of Boron/Epoxy with Fiber orientation angle for different boundary conditions (a) Fix-Fix, (b) Fix-all

Variations of safety factor with Material Types for different boundary conditions are illustrated in Figure 4.8. The Figure 4.8(a) shows that Graphite/Epoxy has the highest safety factor value for fix-fix boundary condition. $[(0/90)_2]_s$, fiber orientation has the highest value for all material types.

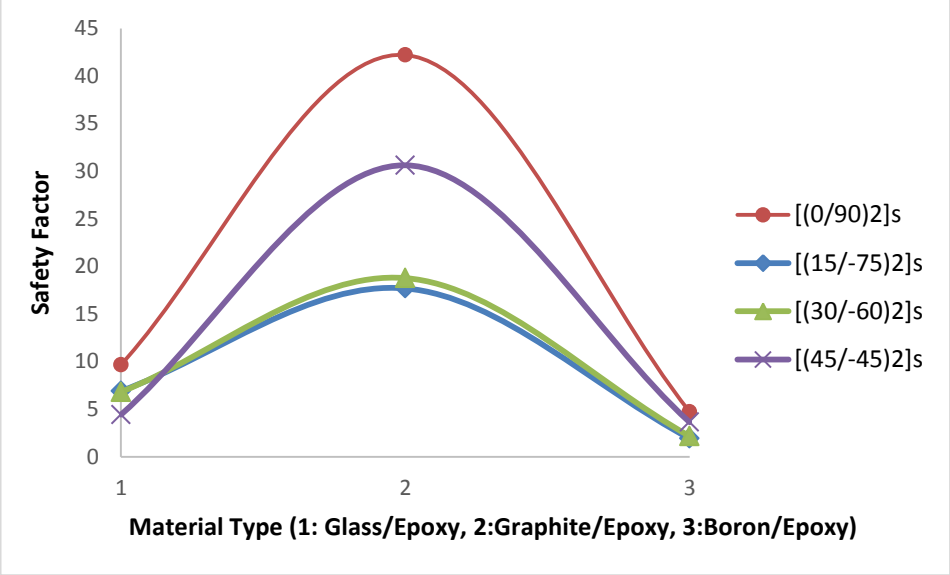

(a)

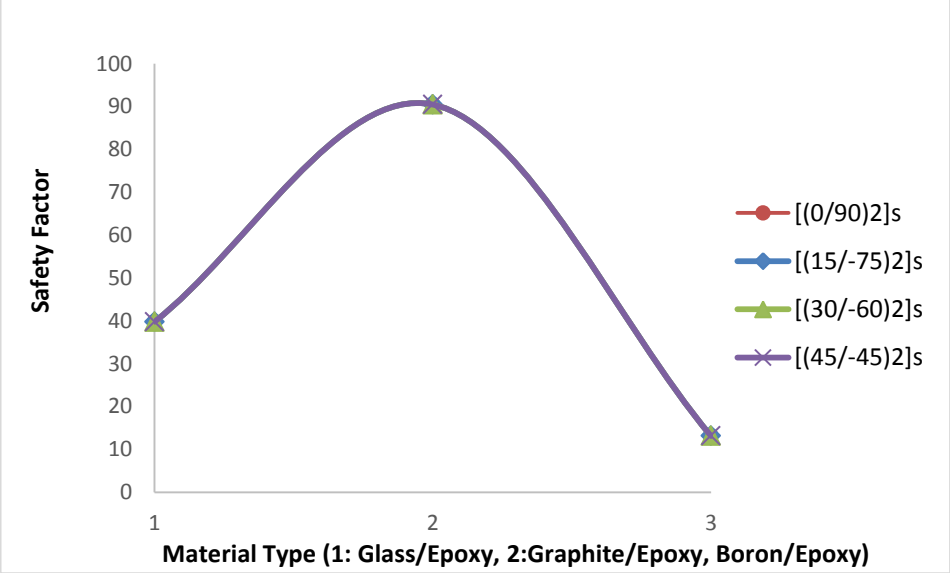

(b)

Figure 4.8 Variation of safety factor with Material Types for different boundary conditions (a) Fix-Fix, (b) Fix-all

4.3 Case 2 (Pure Thermal Fatigue with Cutouts)

In this section, behavior of polymer matrix composites under the thermal fatigue loads that contain different cut-outs are presented. The cut-outs are opened to see

effects of stress concentration on the thermal fatigue resistance of the fiber reinforced composites.

Figure 4.9and 4.10 shows safety factor values for Glass/Epoxy $[(0/90)_2]_s$ fiber orientation with circular cutout for fix-fix boundary condition under pure thermal fatigue with different cutout sizes. As seen in the figure the minimum safety factor value for the circular cutout is increased nearly 13.4 % when the cutout size (A) is increased 30 mm from 10 mm.

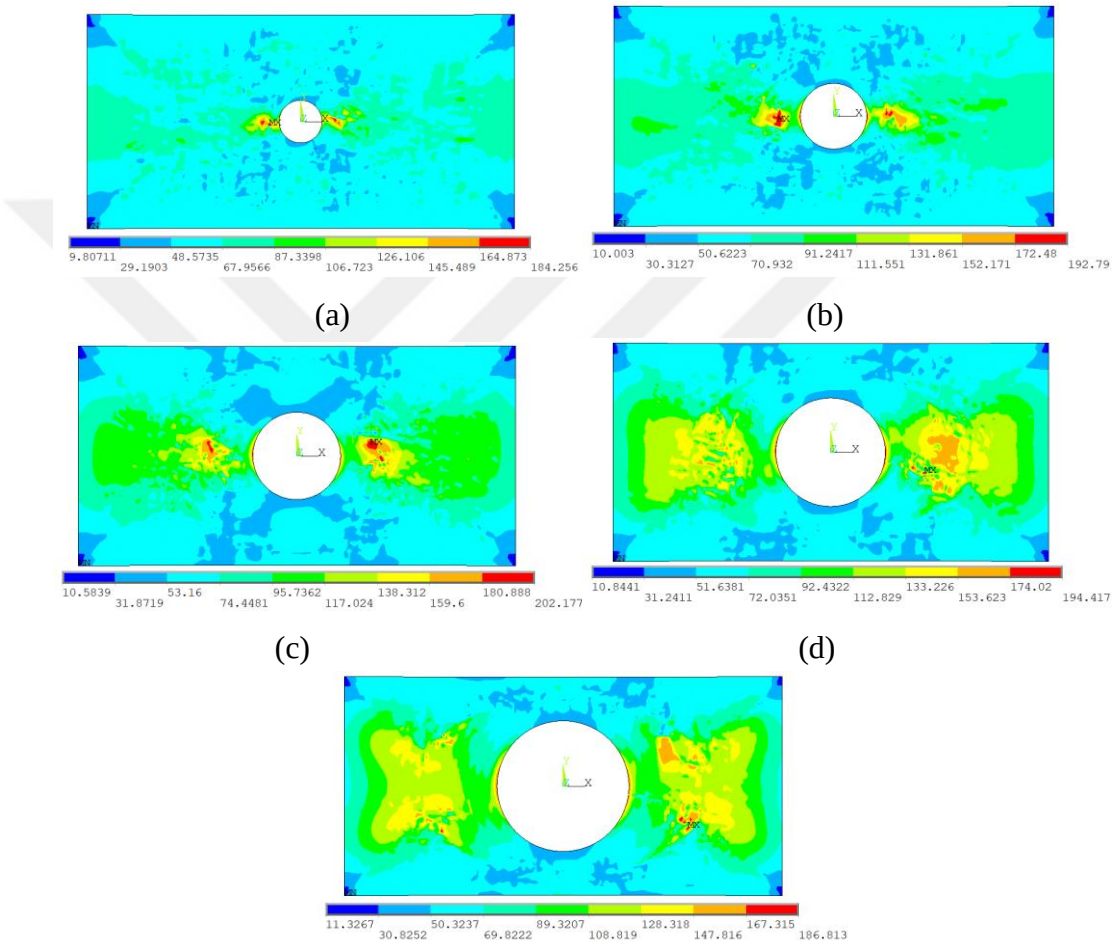

Figure 4.9 Safety factor distribution of Glass/Epoxy $[(0/90)_2]_s$ fiber orientation with circular cutout for fix-fix boundary condition under pure thermal fatigue with different cutout sizes (a)10, (b)15, (c)20, (d)25, (e) 30

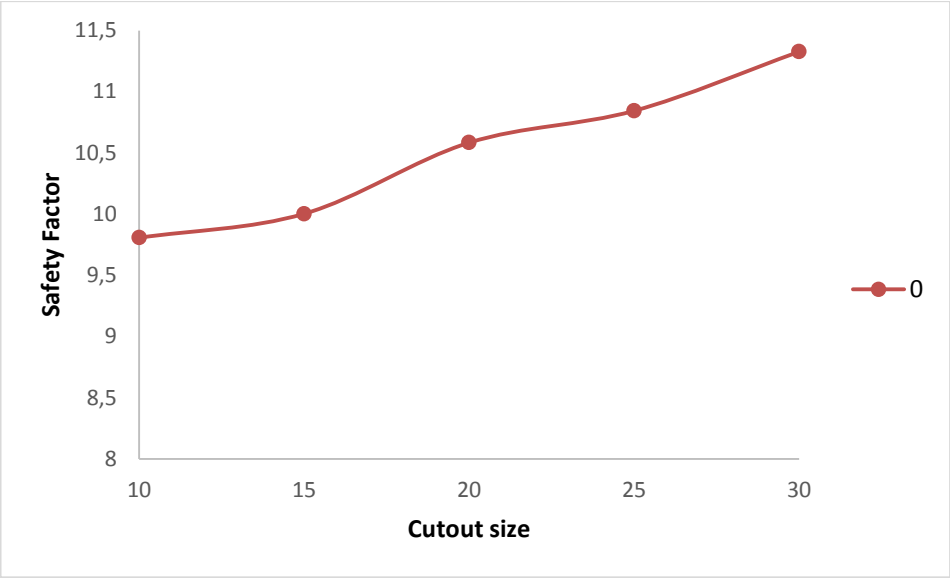

Figure 4.10 Variation of Glass/Epoxy $[(0/90)_2]_s$ fiber orientation with circular cutout for fix-fix boundary condition

Comparison of Safety factor of Glass/Epoxy for circular 20 mm cut-out and with different fiber orientation angles for fix-fix boundary condition are given in Figure 4.11 and 4.12. The safety factor value is higher for $[(0/90)_2]_s$ fiber orientation and minimum for the $[3(0/-60)_2]_s$ fiber orientation.

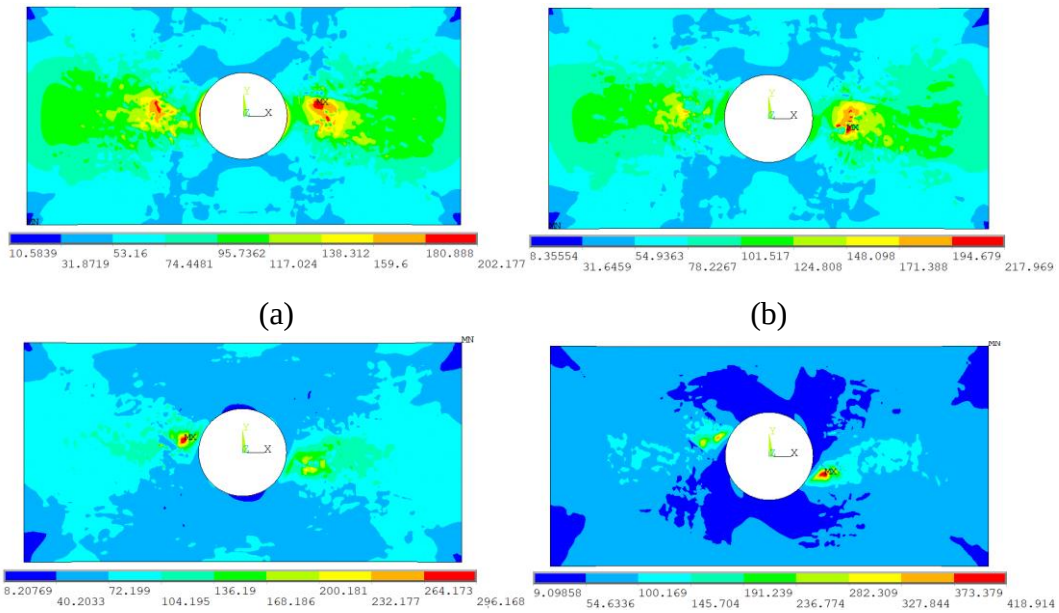

Figure 4.11 Safety factor distribution of Glass/Epoxy for circular 20 mm cut-out and with different fiber orientation angles (a) $[(0/90)_2]_s$**,** (b**)** $[(15/-75)_2]_s$, (c) $[(30/-60)_2]_s$**,** (d) $[(45/-45)_2]_s$**.**

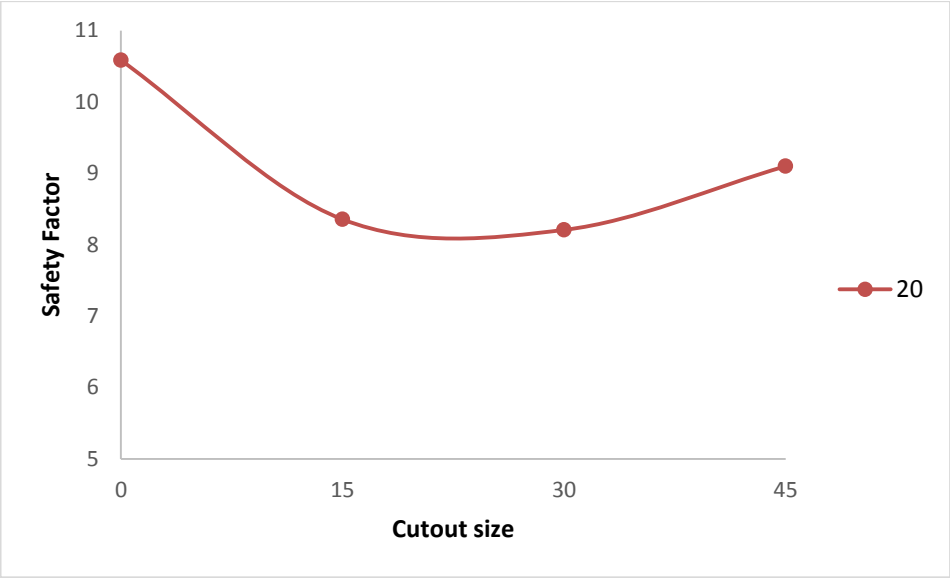

Figure 4.12 Variation of safety factor of Glass/Epoxy for circular 20 mm cut-out and with different fiber orientation angles

Figure 4.13 and 4.14 shows safety factor values for Glass/Epoxy $[(0/90)_2]_s$ fiber orientation with circular cutout for fix-all boundary condition under pure thermal fatigue with different cutout sizes. As seen in the figure the minimum safety factor value for the circular cutout is increased nearly 25.7 % when the cutout size (A) is increased 25 mm from 10 mm. After 25 mm, it stars to decrease.

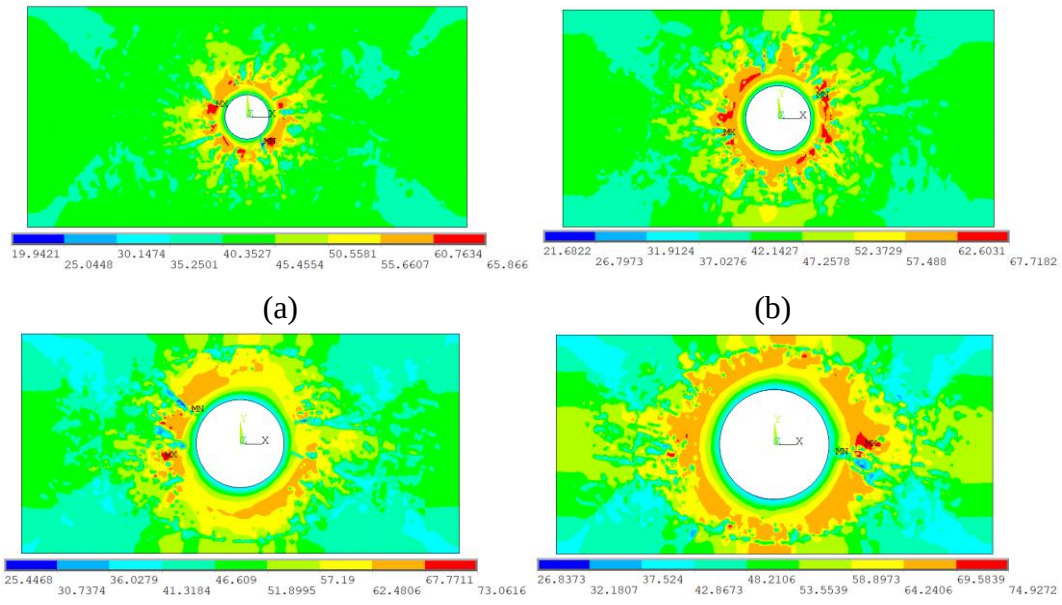

(a) (b)

(c) (d)

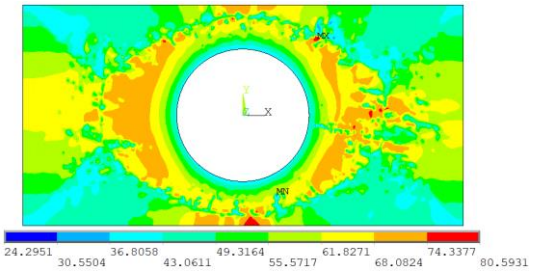

(e)

Figure 4.13 Safety factor distribution of Glass/Epoxy $[(0/90)_2]_s$ fiber orientation with circular cutout for fix-all boundary condition under pure thermal fatigue with different cutout sizes (a)10, (b)15, (c)20, (d)25, (e) 30

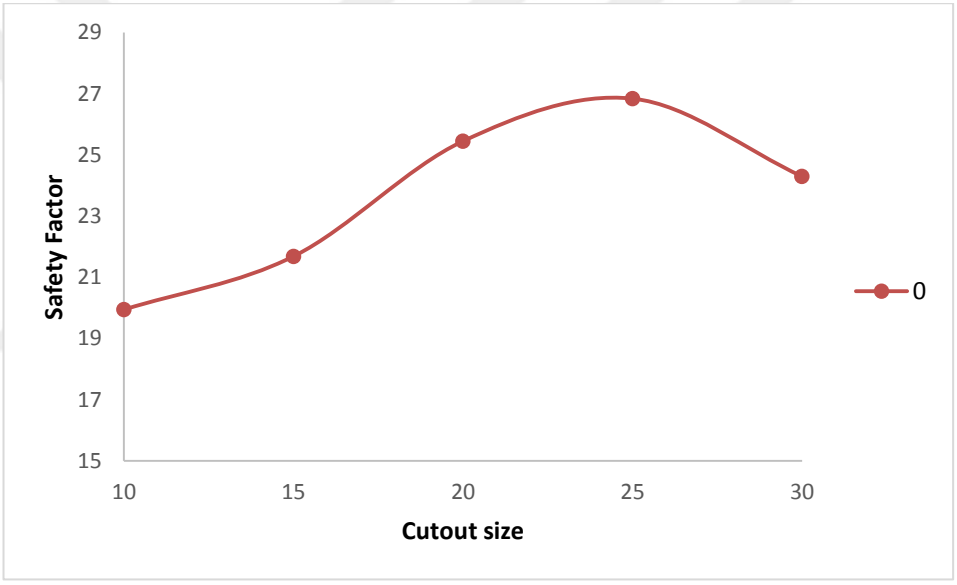

Figure 4.14 Variation of safety factor of Glass/Epoxy for circular 20 mm cut-out and with different cut-out sizes.

Safety factor distribution of Glass/Epoxy with $[(0/90)_2]_s$ fiber orientation for circular 20 mm cut-out and with different cutout positions are given in Figure 4.15. As seen the figures, factor of safety has the highest value when cut-out is at the center.

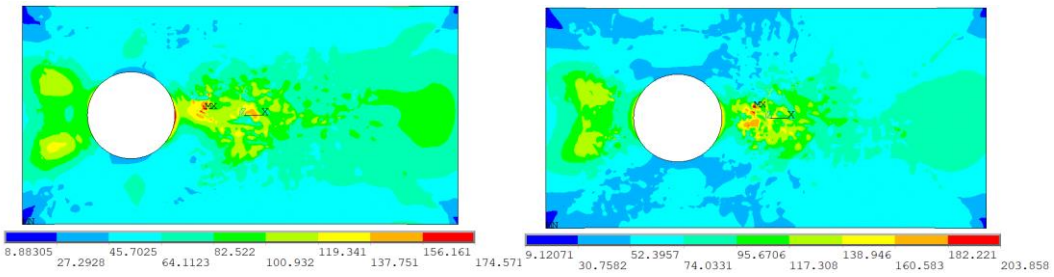
8.88305
27.2928
45.7025
64.1123
82.522
100.932
119.341
137.751
156.161
174.571
9.12071
30.7582
52.3957
74.0331
95.6706
117.308
138.946
160.583
182.221
203.858

(a) (b)

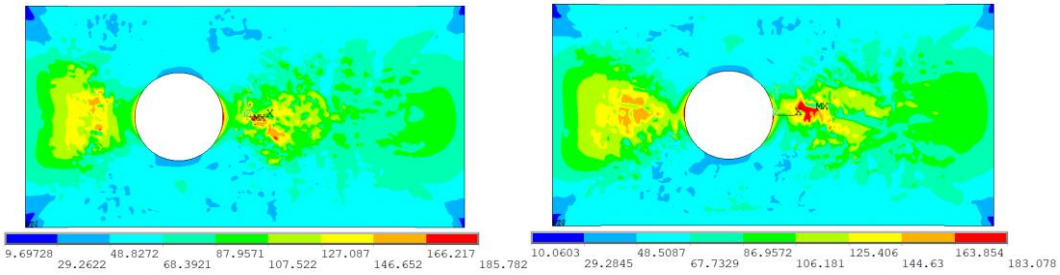
9.69728
29.2622
48.8272
68.3921
87.9571
107.522
127.087
146.652
166.217
185.782
10.0603
29.2845
48.5087
67.7329
86.9572
106.181
125.406
144.63
163.854
183.078

(c) (d)

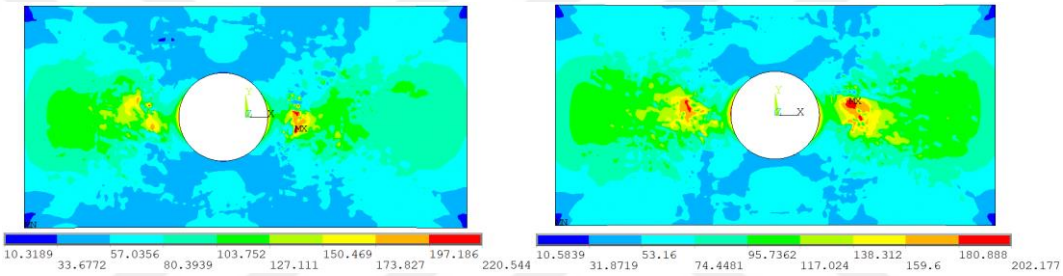
10.3189
33.6772
57.0356
80.3939
103.752
127.111
150.469
173.827
197.186
220.544
10.5839
31.8719
53.16
74.4481
95.7362
117.024
138.312
159.6
180.888
202.177

(e) (f)

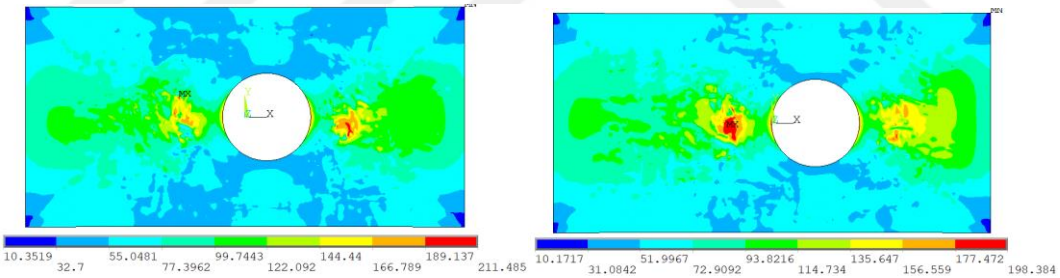
10.3519
32.7
55.0481
77.3962
99.7443
122.092
144.44
166.789
189.137
211.485
10.1717
31.0842
51.9967
72.9092
93.8216
114.734
135.647
156.559
177.472
198.384

(g) (h)

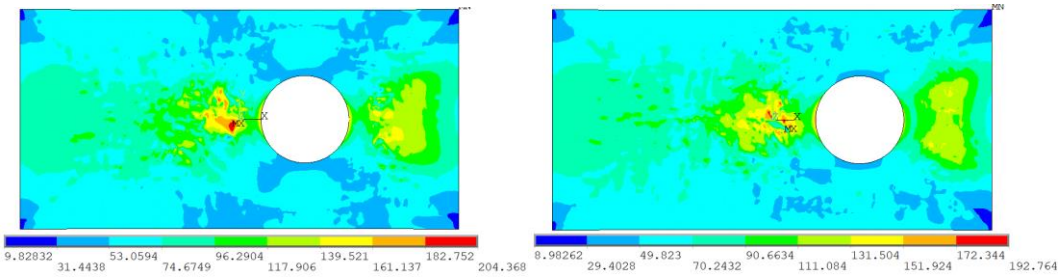
9.82832
31.4438
53.0594
74.6749
96.2904
117.906
139.521
161.137
182.752
204.368
8.98262
29.4028
49.823
70.2432
90.6634
111.084
131.504
151.924
172.344
192.764

(i) (j)

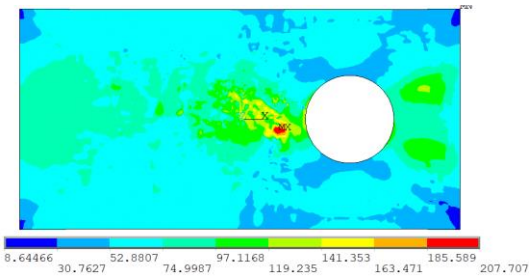

(k)

Figure 4.15 Safety factor distribution of Glass/Epoxy with $[(0/90)_2]_s$ fiber orientation with fix-fix boundary conditions for circular 20 mm cut-out and with different cutout positions (a)-25, (b) -20, (c) -15, (d)-10, (e) -5, (f) 0, (g) 5, (h)10, (i)15, (j) 20, (k) 25

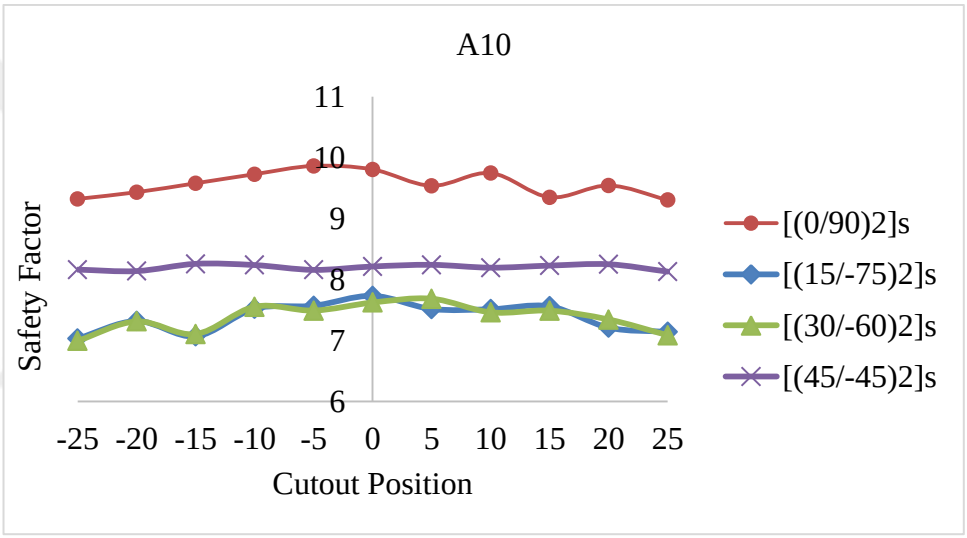

(a)

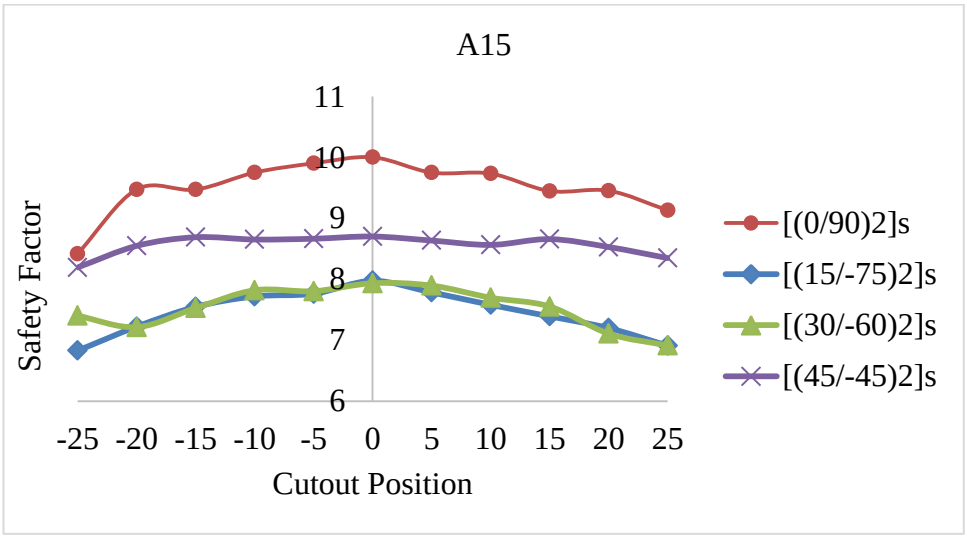

(b)

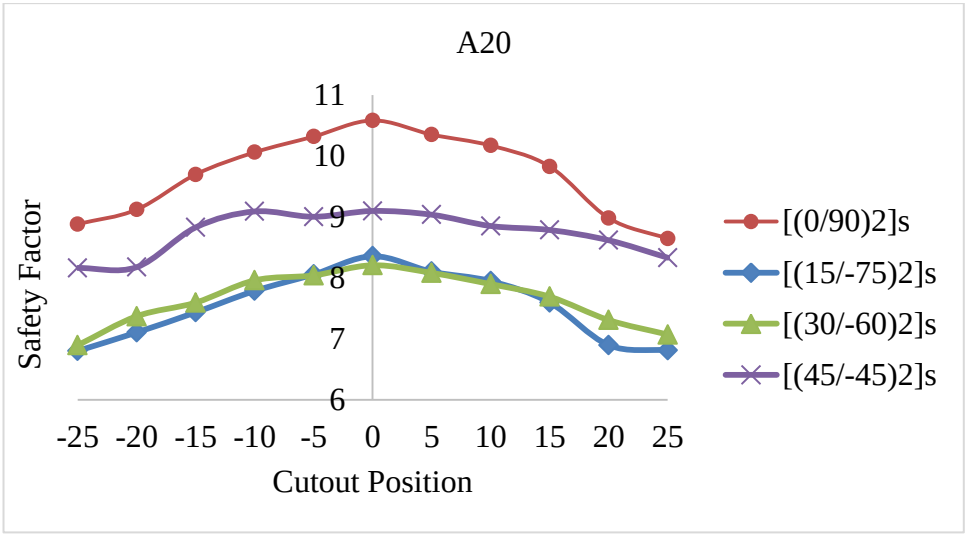
A20
11
10
9
8
7
6
Safety Factor
-25 -20 -15 -10 -5 0 5 10 15 20 25
Cutout Position
[(0/90)2]s
[(15/-75)2]s
[(30/-60)2]s
[(45/-45)2]s

(c)

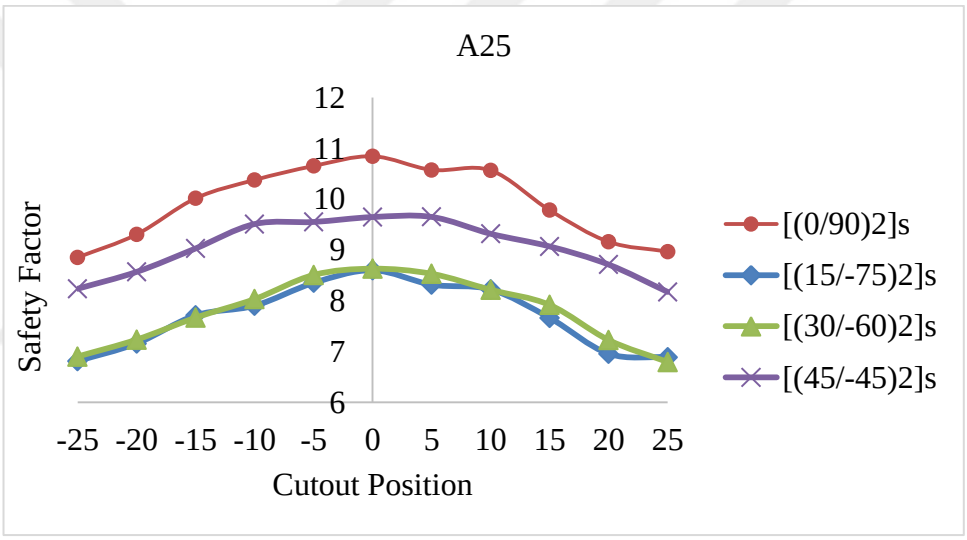
A25
12
11
10
9
8
7
6
Safety Factor
-25 -20 -15 -10 -5 0 5 10 15 20 25
Cutout Position
[(0/90)2]s
[(15/-75)2]s
[(30/-60)2]s
[(45/-45)2]s

(d)

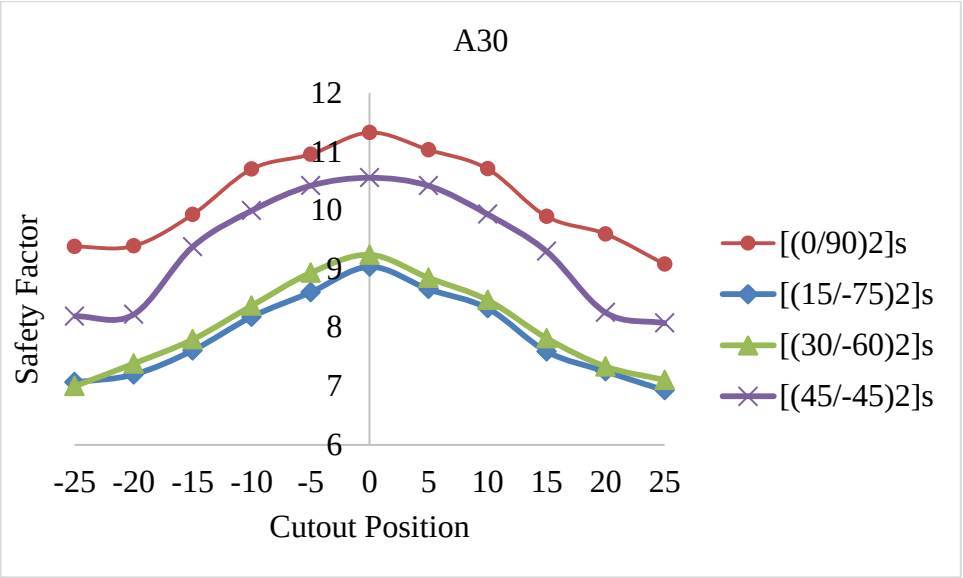

(e)

Figure 4.16 Variation of safety factor of Glass/Epoxy with $[(0/90)_2]_s$ fiber orientation with fix-fix boundary conditions for circular 20 mm cut-out and with different cutout positions for different sizes (a)10, (b)15, (c)20, (d)25, (e) 30

CHAPTER 5

CONCLUSION

In this thesis, thermal fatigue behavior of Glass/Epoxy, Graphite/Epoxy, and Boron/Epoxy composites has been investigated. [(0/90)2]s, [(15/-75)2]s, [(30/-60)2]s, and [(45/-45)2]s fiber orientations are used. Effects of two different boundary conditions are also researched.

It is s seen that fiber orientation and boundary conditions directly affect the thermal fatigue resistance. $[(0/90)_2]_s$, ply sequence has the highest safety factor, and [(45/-45)2]s has the lowest safety factor value. The safety factor values of $[(15/-75)_2]_s$, and $[(30/-60)_2]_s$ are between $[(0/90)_2]_s$ and $[(45/-45)_2]_s$ ply sequences. Also, the different cut-outs are opened to see the effects of stress concentration on the thermal fatigue resistance of the fiber-reinforced composites.

Factor of safety distribution for fix-all and fix-fix boundary conditions under pure thermal fatigue load for $[(0/90)_2]_s$ ply orientation are compared for Glass/Epoxy, Graphite/Epoxy and Boron/Epoxy composites. It was concluded that Graphite/Epoxy laminate has the highest factor of safety value and Boron/Epoxy has the minimum factor of safety value. When $[(0/90)_2]_s$, $[(15/-75)_2]_s$, $[(30/-60)_2]_s$, and $[(45/-45)_2]_s$ fiber orientations and ply sequences are compared, it was seen that $[(0/90)_2]_s$, ply sequence has the highest safety factor and $[(45/-45)_2]_s$ has the lowest safety factor value. The safety factor values of $[(15/-75)_2]_s$, and $[(30/-60)_2]_s$ are between $[(0/90)_2]_s$ and $[(45/-45)_2]_s$ ply sequences. For fix-fix boundary conditions and Graphite/Epoxy $[(0/90)_2]_s$, ply sequence has the highest safety factor value as the Graphite/Epoxy. When ply sequences changes to the $[(15/-75)_2]_s$ the safety factor value decreases. But after $[(30/-60)_2]_s$ ply sequences the safety factor value is started to increase.

When different cutout size are compared, it was seen that the minimum safety factor value for the circular cutout is increased nearly 13.4 % for fix-fix boundary

conditions and 25.7 % for fix-all boundary conditions when the cutout size (A) is increased 30 mm from 10 mm.

Position of the cutout on the plate also has effects on thermal fatigue resistance for all fiber orientations. It is seen that the safety factor increases when the cutout opened at the center of the plate for all orientations. When the cutout is positioned other left side or right side of the plate safety factor begins to decreases with respect to being at the center.

REFERENCES

[1] Yeter, E. (2018) Thermal Fatigue Analyses of Riveted Structures. *Mechanics*. **24(5),** 689-694.

[2] Yeter, E. (2018). Thermal Fatigue Characteristics of Materials Used ın Aerospace Structures. *Energy, Ecology and Environment*. **3(1)**, 24-31.

[3] Yeter, E and Özer, L (2017). Thermal Fatigue Characteristics of Plates with Cutouts, *The International Advanced Researches Engineering Congress.*

[4] Özer, L. (2017) Determination of Thermal Fatigue Characteristics of Thin Plates.

[5] Tian, X., Zhao, J., Wang, X., Yang, H., & Wang, Z. (2018). Performance of Si3N4/(W, Ti) C Graded Ceramic Tool ın High-Speed Turning Iron-Based Superalloys. *Ceramics International*. **44(13)** ,15579-15587.

[6] Wu, C. L., & Han, G. W. (2006). Thermal Fatigue Behaviour of Sicp/Al Composite Synthesized by Metal Infiltration. *Composites Part A: Applied Science and Manufacturing*, **37(11),** 1858-1862.

[7] Li, H., Hu, Y., Liu, C., Zheng, X., Liu, H., & Tao, J. (2016). The Effect of Thermal Fatigue on The Mechanical Properties of The Novel Fiber Metal Laminates Based on Aluminum–Lithium Alloy. *Composites Part A: Applied Science and Manufacturing*. **84,** 36-42.

[8] Li, H., Hu, Y., Fu, X., Zheng, X., Liu, H., & Tao, J. (2016). Effect of Adhesive Quantity on Failure Behavior and Mechanical Properties of Fiber Metal Laminates Based on The Aluminum–Lithium Alloy. *Composite Structures*. **152** ,687-692.

[9] Longbiao, L. (2016). Comparison of Cyclic Fatigue Behavior Between C/Sic and Sic/Sic Ceramic-Matrix Composites at Elevated Temperatures Using Hysteresis Dissipated Energy. *Composite Structures*.**150**, 687-692.

[10] Sarasini, F., Tirillò, J., Valente, M., Ferrante, L., Cioffi, S., Iannace, S., & Sorrentino, L. (2013). Hybrid Composites Based on Aramid and Basalt Woven Fabrics: Impact Damage Modes and Residual Flexural Properties. Materials & Design. **49**, 290-302.

[11] Kobayashi, S., Terada, K., & Takeda, N. (2003). Evaluation of Long-Term Durability ın High Temperature Resistant CFRP Laminates Under Thermal Fatigue Loading. *Composites Part B: Engineering*.**34(8)**, 753-759.

[12] Bieniaś, J., & Dadej, K. (2020). Fatigue Delamination Growth of Carbon and Glass Reinforced Fiber Metal Laminates ın Fracture Mode II. *International Journal of Fatigue*. **130**, 105267.

[13] Shan, Y., Fu, Q., Wen, S., Li, H., & Li, K. (2014). Improvement ın Thermal Fatigue Behavior of Si–Mo–Cr Coated C/C Composites Through Modification of the C/C-Coating Interface. *Surface and Coatings Technology*. **258**, 114-120.

[14] Yan, K. F., Zhang, C. Y, Qiao, S. R., Li, M., & Han, D. (2011). Failure and Strength of 2D-C/Sic Composite Under In-Plane Shear Loading at Elevated Temperatures. *Materials & Design*. **32(6),** 3504-3508.

[15] Tian, C., Liu, N., & Lu, M. (2008). Thermal Shock and Thermal Fatigue Behavior of Si3N4–Tic Nano-Composites. *International Journal of Refractory Metals and Hard Materials*. **26(5),** 478-484.

[16] Zheng, G., Zhao, J., Gao, Z., & Cao, Q. (2012). Cutting Performance and Wear Mechanisms of Sialon–Si 3 N 4 Graded Nano-Composite Ceramic Cutting Tools. *The International Journal of Advanced Manufacturing Technology*.**58(1-4),** 19-28.

[17] Colombo, C., Vergani, L. A. U. R. A., & Burman, M. (2012). Static and Fatigue Characterisation of New Basalt Fibre Reinforced Composites. *Composite Structures.* **94(3),** 1165-1174.

[18] Wong, E. H., Lim, K. M., & Mai, Y. W. (2009). Analytical Solutions for PCB Assembly Subjected to Mismatched Thermal Expansion. *IEEE Transactions on Advanced Packaging*.**32(3)**, 602-611.

[19] Chen, X., Peng, X., Wei, Z., Yue, X., & Fu, T. (2017). Effect of Tensile Stress on Thermal Fatigue Life of Zrb2-Sic-Graphite Composite. *Materials & Design*. **126,** 91-97.

[20] Longbiao, L. (2017). Modeling Strength Degradation of Fiber-Reinforced Ceramic-Matrix Composites Under Cyclic Loading at Room and Elevated Temperatures. *Materials Science and Engineering: A.* **695**, 221-229.

[21] Zhou, Y., Wei, S., Wang, L., Xu, L., Li, X., & Pan, K. (2020). Study on Thermal Fatigue Performance of The Molybdenum Plate Doped with Al2O3 Particles. Journal of Alloys and Compounds. **823**, 153748.

[22] Kobayashi, S., Terada, K., & Takeda, N. (2003). Evaluation of Long-Term Durability ın High Temperature Resistant CFRP Laminates Under Thermal Fatigue Loading. *Composites Part B: Engineering*. **34(8)**, 753-759.

[23] Pan, L., Han, J., Yang, Z., Li, X., Wang, J., Li, Z., & Li, W. (2017). Thermal Fatigue Crack Behavior of Sicp/A356 Composites Prepared by Stirring Casting. *Results ın Physics.* **7**, 927-933.

[24] Longbiao, L. (2019). A Thermomechanical Fatigue Hysteresis-Based Damage Evolution Model for Fiber-Reinforced Ceramic–Matrix Composites. *International Journal of Damage Mechanics.* **28(3)** 380-403.

[25] Mchale, C., Carey, S., Hadjiloizi, D., & Weaver, P. M. (2020). Morphing Composite Cylindrical Lattices: *Thermal Effects and Actuation. ın AIAA Scitech 2020 Forum* **(P. 0247).**

[26] Ghasemi, A. R., Tabatabaeian, A., & Asghari, B. (2019). Application of Slitting Method to Characterize the Effects of Thermal Fatigue, Lay-Up Arrangement and Mwcnts on The Residual Stresses of Laminated Composites. *Mechanics of Materials*. **134**, 185-192.

[27] Li, W., Cho, Y., & Achenbach, J. D. (2012). Detection of Thermal Fatigue ın Composites by Second Harmonic Lamb Waves. *Smart Materials and Structures*. **21(8)**, 085019.

[28] Li, Z., Jiang, Y., Zhou, R., Gao, F., Shan, Q., & Tan, J. (2014). Thermal Fatigue Mechanism of WC Particles Reinforced Steel Substrate Surface Composite at Different Thermal Shock Temperatures. *Journal of Alloys and Compounds*. **596**, 48-54.

[29] Li, W., Xu, C., & Cho, Y. (2016). Characterization of Degradation Progressive ın Composite Laminates Subjected to Thermal Fatigue and Moisture Diffusion by Lamb Waves. *Sensors*. **16(2)**, 260.

[30] Pieniak, D., Przystupa, K., Walczak, A., Niewczas, A. M., Krzyzak, A., Bartnik, G., & Lonkwic, P. (2019). Hydro-Thermal Fatigue of Polymer Matrix Composite Biomaterials. *Materials*.**12(22)**, 3650.

[31] Ghasemi, A. R., Tabatabaeian, A., & Asghari, B. (2019). Application of Slitting Method to Characterize the Effects of Thermal Fatigue, Lay-Up Arrangement and Mwcnts on The Residual Stresses of Laminated Composites. *Mechanics of Materials*. **134**, 185-192.

[32] Wu, C. L., & Han, G. W. (2006). Thermal Fatigue Behaviour of Sicp/Al Composite Synthesized by Metal Infiltration. Composites Part A: Applied Science and Manufacturing. **37(11)**, 1858-1862.

[33] Zheng, G., Zhao, J., Jia, C., Tian, X., Dong, Y., & Zhou, Y. (2012). Thermal Shock and Thermal Fatigue Resistance of Sialon–Si3N4 Graded Composite Ceramic Materials. *International Journal of Refractory Metals and Hard Materials.* **35**, 55-61.

[34] Prakash, V. A., Xavier, J. F., Ramesh, G., Maridurai, T., Kumar, K. S., & Raj, R. B. S. (2020). Mechanical, Thermal and Fatigue Behaviour of Surface-Treated Novel Caryota Urens Fibre–Reinforced Epoxy Composite. *Biomass Conversion and Biorefinery*, **1(11).**

[35] Schöbel, M., Degischer, H. P., Vaucher, S., Hofmann, M., & Cloetens, P. (2010). Reinforcement Architectures and Thermal Fatigue ın Diamond Particle-Reinforced Aluminum. *Acta Materialia.* **58(19)**, 6421-6430.

[36] Bahramian, A. R., Kokabi, M., Famili, M. H. N., & Beheshty, M. H. (2006). Ablation and Thermal Degradation Behaviour of a Composite Based on

Resol Type Phenolic Resin. *Process Modeling and Experimental. Polymer*. **47(10)**, 3661-3673.

[37] Bellenger, V., Tcharkhtchi, A., & Castaing, P. (2006). Thermal and Mechanical Fatigue of a PA66/Glass Fibers Composite Material. *International Journal of Fatigue*. **28(10)**, 1348-1352.

[38] Chen, N., Zhang, H., Gu, M., & Jin, Y. (2009). Effect of Thermal Cycling on the Expansion Behavior of Al/Sicp Composite. *Journal of Materials Processing Technology*. **209(3)**, 1471-1476.

[39] Fei, W. D., Hu, M., & Yao, C. K. (2003). Thermal Expansion and Thermal Mismatch Stress Relaxation Behaviors of Sic Whisker Reinforced Aluminum Composite. *Materials Chemistry and Physics*. **77(3)**, 882-888.

[40] Ferreira, J. A. M., Reis, P. N., Costa, J. D. M., & Richardson, M. O. W. (2002). Fatigue Behaviour of Composite Adhesive Lap Joints. *Composites Science and Technology*. **62(10-11)**, 1373-1379.

[41] Giannadakis, K., & Varna, J. (2009, September). Effect of Thermal Aging and Fatigue on Failure Resistance of Aerospace Composite Materials. In IOP Conference Series. *Materials Science and Engineering* **(5).**

[42] Hosseini-Toudeshky, H., & Mohammadi, B. (2009). Thermal Residual Stresses Effects on Fatigue Crack Growth of Repaired Panels Bounded with Various Composite Materials. *Composite Structures*. **89(2)**, 216-223.

[43] Jeyaraj, P., Padmanabhan, C., & Ganesan, N. (2008). Vibration and Acoustic Response of an Isotropic Plate a Thermal Environment. *Journal of Vibration and Acoustics*, **130(5).**

[44] Ju, J., & Morgan, R. J. (2004). Characterization of Microcrack Development ın BMI-Carbon Fiber Composite Under Stress and Thermal Cycling. *Journal of Composite Materials*. **38(22)**, 2007-2024.

[45] Levy-Tubiana, R., Baczmanski, A., & Lodini, A. (2003). Relaxation of Thermal Mismatch Stress Due to Plastic Deformation ın an Al/Sicp Metal Matrix Composite. *Materials Science and Engineering.* **A, 341(1-2),** 74-86.

[46] Mehrman, J. M., Ruggles-Wrenn, M. B., & Baek, S. S. (2007). Influence of Hold Times on The Elevated-Temperature Fatigue Behavior of an Oxide–Oxide Ceramic Composite ın Air and In Steam Environment. *Composites Science and Technology*. **67(7-8)**, 1425-1438.

[47] Nousiainen, O., Kangasvieri, T., Rautioaho, R., & Vähäkangas, J. (2009). Thermal Fatigue Endurance of Lead-Free Composite Solder Joints Over a Temperature Range of− 55 C to 150 C. *Journal of Electronic Materials*. **38(6)**, 843-851.

[48] Petit, S., Bouvet, C., Bergerot, A., & Barrau, J. J. (2007). Impact and Compression After Impact Experimental Study of a Composite Laminate with a Cork Thermal Shield. *Composites Science and Technology*. **67(15-16)**, 3286-3299.

[49] Ray, B. C. (2005). Thermal Shock and Thermal Fatigue on Delamination of Glass-Fiber-Reinforced Polymeric Composites. *Journal of Reinforced Plastics and Composites*. **24(1)**, 111-116.

[50] Shariyat, M. (2007). Thermal Buckling Analysis of Rectangular Composite Plates with Temperature-Dependent Properties Based on a Layerwise Theory. *Thin-Walled Structures*. **45(4)**, 439-452.

[51] Shimokawa, T., Kakuta, Y., Hamaguchi, Y., & Aiyama, T. (2008). Static and Fatigue Strengths of a G40-800/5260 Carbon Fiber/Bismaleimide Composite Material at Room Temperature And 150 C. *Journal of Composite Materials*. **42(7)**, 655-679.

[52] Tingzhi, S. I., Ning, L. I. U., & Xianqing, Y. O. U. (2008). Thermal Shock Fatigue Behavior of Tic/Al2O3 Composite Ceramics. *Rare Metals*. **27(3)**, 308-314.

[53] Sobczak, J., Sobczak, N., Darlak, P., Slawinski, Z., Asthana, R., & Rohatgi, P. (2002). Thermal Fatigue Resistance of Discontinuously Reinforced Cast Aluminum-Matrix Composites. *Journal of Materials Engineering and Performance*. **11(6)**, 595.

[54] ASM International Handbook Committee (1996). Fatigue and Fracture. *United States of America.*

[55] I. Göv, (2014). Applying Topology Optimization to 3d Machine Parts Under Static and Fatigue Loading. *Turkey.*

[56] D.A Sphere, D.F Mowbray (1975). Thermal Fatigue of Materials and Components. *Philadelphia.*

[57] ANSYS Manual Book.

[58] Kaw, A. K. (2005). Mechanics of Composite Materials. *CRC Press.*